Thyroid Hormone Receptor α Regulates Autophagy, Mitochondrial Biogenesis, and Fatty Acid Use in Skeletal Muscle

Jin Zhou, Karine Gauthier, Jia Pei Ho, Andrea Lim, Xu-Guang Zhu, Cho Rong Han, Rohit Anthony Sinha, Sheue-Yann Cheng, Paul Michael Yen

Thyroid hormone receptor-α regulates autophagy, mitochondrial biogenesis, and fatty acid utilization in skeletal muscle

Jin Zhou[1], Karine Gauthier[2], Jia Pei Ho[1], Andrea Lim[1], Xu-guang Zhu[3], Cho Rong Han[3], Rohit Anthony Sinha[4], Sheue-Yann Cheng[3], Paul Michael Yen[1,5,6]

[1]Program of Cardiovascular and Metabolic Disorders, Duke-NUS Medical School Singapore, Singapore
[2]Institut de Genomique Fonctionnelle de Lyon, Universite de Lyon, France
[3]Laboratory of Molecular Biology, Center for Cancer Research, National Cancer Institute, Bethesda, Maryland, USA
[4]Department of Endocrinology, Sanjay Gandhi Postgraduate Institute of Medical Sciences, Lucknow-226014, India
[5]Duke Molecular Physiology Institute, Durham, NC 27701, USA
[6]Duke University School of Medicine, Durham, NC 27710, USA

Short title: TRα1 mutation impairs muscle autophagy

Key words: TRα1 mutation; autophagy; mitochondrial function; lipid metabolism; muscle

To whom correspondence should be sent: Jin Zhou (jin.zhou@duke-nus.edu.sg) or Paul M. Yen (paul.yen@duke-nus.edu.sg), Program of Cardiovascular & Metabolic Disorders, Duke-NUS Medical School, 8 College Road, Singapore 169857

Declaration: The authors declare no conflict of interest.

Data Availability Statement: Supplementary Figures (1) can be found: Thyroid hormone receptor alpha regulates autophagy, mitochondrial biogenesis, and fatty acid utilization in skeletal muscle. Figshare. Deposited on 29 March 2021.
https://figshare.com/s/78918d8bb5a44f1d3f24; DOI: 10.6084/m9.figshare.14331599.

Abstract

Skeletal muscle (SM) weakness occurs in hypothyroidism and resistance to thyroid hormone alpha (RTHα) syndrome. However, the cell signaling and molecular mechanism(s) underlying muscle weakness under these conditions is not well understood. We thus examined the role of thyroid hormone receptor alpha (TRα), the predominant TR isoform in SM, on autophagy, mitochondrial biogenesis and metabolism to demonstrate the molecular mechanism(s) underlying muscle weakness in these two conditions.

Two genetic mouse models, *TRα1*$^{PV/+}$ mice which expresses mutant Thra1PV gene ubiquitously, and *SM-TRα1*$^{L400R/+}$ mice, which expresses *TRα1*^{L400R} in a muscle-specific manner, were used in this study. Gastrocnemius muscle from *TRα1*$^{PV/+}$, *SM-TRα1*$^{L400R/+}$, and their control mice was harvested for analyses.

We demonstrated that loss of TRα1 signaling in gastrocnemius muscle from both the genetic mouse models led to decreased autophagy as evidenced by accumulation of p62 and decreased expression of lysosomal markers (LAMP1, and LAMP2) and lysosomal proteases (cathepsin B and cathepsin D). The expression of PGC1α, TFAM, and ERRα, key factors contributing to mitochondrial biogenesis as well as mitochondrial proteins were decreased, suggesting that there was reduced mitochondrial biogenesis due to the expression of mutant TRα1. Transcriptomic and metabolomic analyses of SM suggested that lipid catabolism was impaired, and was associated with decreased acylcarnitines and tricarboxylic acid cycle (TCA cycle) intermediates in the SM from the mouse line expressing SM-specific mutant TRα1. Our results provide new insight into TRα1-mediated cell signaling, molecular, and metabolic changes that occur in SM when TR action is impaired.

Introduction

Hypothyroidism is a common chronic condition that can occur in as many as 5% of the adult population in some countries (2,3). Patients with hypothyroidism have decreased resting energy expenditure and muscle strength (4,5). Additionally, thyroid hormone (TH) has profound effects on SM architecture, metabolism, contractile function, myogenesis and regeneration (6-8). Interestingly, TH stimulates both glycolysis and/or fatty acid β-oxidation in myocytes (9,10). It also induces the transition from slow twitch to fast twitch muscle fibers as well as the metabolic changes associated with that transition (6,10,11). Thus, it can stimulate SM activity based upon muscle fiber type and/or fuel availability. TH also increases autophagy/mitophagy and mitochondrial biogenesis (11). However, the effects of hypothyroidism on these processes is not well understood.

Thyroid hormone receptor alpha1 (TRα1) is the pre-dominant receptor isoform in SM, and is thought to mediate most of TH's actions in SM (12). Animal and human studies on the actions of TH in SM have examined hypo- or hyperthyroidism at the systemic level (13). Thus, little is known about the direct effects of TH on transcription, metabolism, and mitochondria on SM *in vivo* when its actions are impaired during hypothyroidism or resistance to thyroid hormone alpha (RTHα). Patients with RTHα have been reported to harbor TRα mutations, (TRa1E403X, TRa1F397fs406X, or TRa1A397PfsX7) (14-16). Although patients were heterozygotes, they exhibited classical features of hypothyroidism in tissues that expressed high levels of TRα such as heart, skeletal muscle, and bone (14-16). Furthermore, these mutations exhibited dominant negative action and interfered with the transcriptional activity of wildtype TRα (14-16). The isoform-specific role of TRα1 on metabolism and mitochondrial activity has been examined in several tissues (12,13) but little is known about TRα1's role in SM. Accordingly, we examined two genetic mouse models in which dominant negative mutant TRα1s were expressed ubiquitously or in a skeletal muscle-specific manner. These mutant TRα1s both had impaired hormone binding to TH, decreased transcriptional activity, and dominant negative activity on

normal TRα isoforms (17,18). These abnormalities due to mutant TRα1 were not rescued by TH administration (19). We examined the effects of inhibiting TRα1 activity on SM on autophagy, mitochondrial turnover, lipid metabolism, and muscle fiber phenotype to better understand the molecular pathogenesis underlying the impaired energy metabolism observed in SM of patients with hypothyroidism and RTHα syndrome.

Materials and Methods

Animal models

TRα$^{AMI/+}$ mice were generated and genotyped as described earlier (18). *TRα*$^{AMI/+}$ mice allow the conditional expression of a TRα1 point mutant, in which the leucine present in the AF2 is converted into an arginine (L400R). The *TRα1*^{L400R} reading frame flanked by the upstream *PGKNeoRpolyA* and the downstream *IRESTaulacZ* cassettes, was introduced in the mouse *THRA* locus by homologous recombination under its natural promoter. The upstream *PGKNeoRpolyA* cassette contains a simian virus 40 (SV40) polyadenylation signal, which arrests most transcription and prevents any TRα1^{L400R} translation. Because the upstream *PGKNeoRpolyA* cassette is flanked by two tandem *loxP* sequences, the expression of *TRα*^{AMI} allele was induced only after CRE/loxP-mediated DNA recombination (18). To generate muscle-specific *TRα*$^{AMI/+}$ mice (referred as *SM-TRα1*$^{L400R/+}$ mice thereafter), *TRα*$^{AMI/+}$ mice then were crossed with human skeletal actin (HSA)-cre mice, which enabled the expression of *TRα1*^{L400R} specifically in the muscle, while the *TRα*$^{AMI/+}$ mice served as control (referred as *Control* thereafter). Three to five-month old male mice were used for this study. This animal study was carried out in accordance with the European Community Council Directive of September 22, 2010 (2010/63/EU) regarding the protection of animals used for experimental and other scientific purposes. The research project was approved by a local animal care and use committee (C2EA015) in Lyon and subsequently authorized by the French Ministry of Research.

Mice harbouring the mutant Thra1PV gene (*TRα1*$^{PV/+}$ mice) and *wild-type* littermates were prepared and genotyped as described earlier (17). Three to four month old female mice were

used for this study.This animal study was carried out according to the protocol approved by the National Cancer Institute Animal Care and Use Committee.

Animals were housed in hanging polycarbonate cages under a 12-hour light/12-hour dark cycle at 23°C with food and water available ad libitum. Animals were sacrificed in CO2 chambers and gastrocnemius muscle were collected in liquid N2 and subsequently used for protein isolation.

Western Blot

A total of 20–40 mg gastrocnemius muscle were used to generate protein lysate, and the following western blotting procedure was performed as described (10). Visualization was performed using the enhanced chemiluminescence system (GE Healthcare). Densitometric analyses of western blot images were performed by using Image J software (NIH, Bethesda, MD, United States). Phosphorylated protein was normalized to total protein, and others were normalized to GAPDH or β-actin. Antibodies information listed in Supplementary Table 1(1).

RNA-seq and pathway analysis

RNA was isolated from gastrocnemius muscle tissue using QIAzol (Qiagen, Hilden, Germany), followed by clean-up using Invitek Mini Kit (Invitek, San Francisco, CA) following the manufacturer's protocol. RNA-seq and pathway analysis on pooled samples of each *Control* (n=4) and *SM-TRα1*$^{L400R/+}$ (n=4) was performed by NovogeneAIT Genomics Singapore Pte Ltd. Briefly, Alignments were parsed using Tophat program and differential expressions were determined through DESeq2/edgeR. GO enrichment were implemented by the ClusterProfiler.

Metabolomics

In accordance with previously established mass spectrometry (MS)-based methods, gastrocnemius muscle samples were used for quantitative determination of targeted metabolite levels for acylcarnitine species and organic acids by the Metabolomics Core Facility of Duke-NUS Medical School (10). Muscle tissue was homogenized in 50% acetonitrile and 0.3% formic acid. For acylcarnitine and organic acid extraction, 100 µL of tissue homogenate was extracted

using methanol. The acylcarnitine extracts were derivatized with 3 M hydrochloric acid in methanol, dried, and reconstituted in methanol for analysis in liquid chromatography/mass spectrometry (LC/MS). Organic acid extracts were derivatized to form butyl esters using 3 M HCl in butanol. Samples were then reconstituted in 80% aqueous methanol and 4 µL of this solution was used for analysis. The heatmap of lipidomic profiling was presented as mean value of each group using normalized percentage value for each lipid species, with smallest mean defined as 0%, and largest mean defined as 100%. All the analysis was done using GraphPad Prism 8.

Statistical Analysis

The comparison between *SM-TRα1*$^{L400R/+}$ and *Control* mice, and *TRα1*$^{PV/+}$ mice with its *wild-type* littermates were conducted using unpaired parametric Student's t-test in GraphPad Prism. Statistical significance was declared at a p*p <0.05, **p <0.01, ****p<0.0001.

Results

TRα1 mutation decreased autophagy in gastrocnemius muscle

In the current study, we used two mouse models expressing dominant-negative mutations in TRα1: *SM-TRα1*$^{L400R/+}$ knock-in mice which were heterozygous for a dominant negative *TRα1*^{L400R} point mutation (conversion of a Leucine to an Arginine in the AF2 domain) that was conditionally expressed in SM; and *TRα1*$^{PV/+}$ knock-in mice which were heterozygous for a dominant negative TRα1^{PV} frameshift mutation that was ubiquitously expressed. *TRα1*$^{PV/+}$ mice faithfully recapitulated the phenotype exhibited by patients with mutations of the *THRA* gene (17).

We previously observed that TH stimulated autophagy in SM (11), so we examined autophagy in the gastrocnemius muscle from *SM-TRα1*$^{L400R/+}$ and *Control* mice. The protein levels of LC3B-II and p62 were elevated in *SM-TRα1*$^{L400R/+}$ mice compared to *Controls* (Fig. 1A). Similarly, p62 accumulated in gastrocnemius muscle from *TRα1*$^{PV/+}$ mice (Fig. 1B). Since p62 accumulates

when autophagic flux is decreased (20), the increase in p62 protein levels suggested there was decreased autophagy in both mouse strains. We also assessed p62 level in wildtype C57BL/6 mice injected with normal saline or T_3, and found that T_3 decreased p62 in wildtype mice (Supplementary Fig. 1(1)), confirming that T_3 negatively regulates p62 protein. We next assessed the expression of lysosomal marker proteins such as lysosomal-associated membrane protein 1 (LAMP-1) and lysosomal-associated membrane protein 2 (LAMP-2), and the lysosomal proteases, cathepsin B and cathepsin D. There was decreased expression of these lysosomal proteins in SM from *SM-TRα1*$^{L400R/+}$ mice compared to *Control* mice (Fig. 2A-B). Similar decreases in LAMP1, cathepsin B and cathepsin D protein expression also were seen in SM from *TRα1*$^{PV/+}$ mice (Fig. 2D). We next investigated the phosphorylation of TFEB (Fig. 2C and 2E), a key transcription factor for lysosomal biogenesis genes that is inhibited by mTOR phosphorylation at Ser142 (21). Decreased total TFEB and/or increased phosphorylated TFEB protein levels led to an increased p-TFEB/TFEB ratios that were higher in *SM-TRα1*$^{L400R/+}$ and *TRα1*$^{PV/+}$ mice than controls (Fig. 2C and 2E). Taken together, these results showed that the expression of mutant TRα1 in SM decreased autophagy and decreased lysosomal protein expression.

The mammalian target of rapamycin (mTOR) and AMP-activated protein kinase (AMPK) signaling are two major pathways that control autophagy, and both are regulated by TH (11,22). We found increased phosphorylation of two mTOR targets, eukaryotic translation initiation factor 4E (eIF4E)-binding protein 1 (4EBP1) and p70S6 kinase (p70S6K) (Fig. 3A-C), suggesting an increase in mTOR signaling in the SM from *SM-TRα1*$^{L400R/+}$ mice. There also was decreased phosphorylation of AMPK and adipose triglyceride lipase (ATGL) at Ser406 (Fig. 3D–F), a site that is phosphorylated by AMPK (23) in the SM from *SM-TRα1*$^{L400R/+}$ mice. Similarly, there was increased phosphorylation of 4EBP1 and decreased phosphorylation of ATGL in the SM from *TRα1*$^{PV/+}$ mice (Supplementary Fig. 2(1)). These findings showed that expression of mutant TRα1 in SM led to increased mTOR and decreased AMPK signaling.

TRα1 mutation decreased mitochondrial turnover in gastrocnemius muscle

TH increased mitochondrial turnover by increasing mitophagy and mitochondrial biogenesis (11,22,24). We examined several mitophagy markers in SM from *SM-TRα1*$^{L400R/+}$ and *Control* mice. There was no change in the expression of PINK1; however, protein levels of Drp1 and parkin were decreased in *SM-TRα1*$^{L400R/+}$ mice (Fig. 4), suggesting that mitophagy may have been impaired in *SM-TRα1*$^{L400R/+}$ mice. In SM from *TRα1*$^{PV/+}$ mice, the protein levels of parkin was unchanged but Drp1 was decreased (Supplementary Fig. 3(1)). The decreases in Drp1 expression also suggested that mitochondrial fission might be impaired in both mouse strains. We also assessed Drp1 levels in wildtype C57BL/6 mice injected with normal saline or T_3, and found that T_3 did not affect Drp1 expression in wildtype mice (Supplementary Fig. 4(1)). Thus, it is possible that Drp1 expression is regulated at physiological levels of T_3 but is not further increased during hyperthyroidism.

Peroxisome proliferator-activated receptor gamma coactivator 1-alpha (PGC1α), mitochondrial transcription factor A (TFAM) and estrogen-related receptor alpha (ERRα) are key factors involved in mitochondrial biogenesis (24,25). PGC1α, TFAM, and ERRα protein levels were decreased in the SM from *SM-TRα1*$^{L400R/+}$ mice (Fig. 5A), suggesting that *TRα1*^{L400R} decreased mitochondrial biogenesis. Mitochondrial proteins such as translocase of outer mitochondrial membrane 20 (TOMM20), voltage-dependent anion channel 1 (VDAC1), and cytochrome c oxidase subunit 4I1 (COXIV) also were decreased in *SM-TRα1*$^{L400R/+}$ mice (Fig. 5B-C). Similarly, *TRα1*$^{PV/+}$ mice exhibited decreased protein levels of ERRα, TOMM20, VDAC1 and COXIV in SM (Fig. 5D). These results suggested that mutant TRα1 decreased mitochondrial biogenesis and content in SM.

Dysregulated mitochondrial metabolism in muscle from *SM-TRα1*$^{L400R/+}$ mice

We previously showed that TH increased β-oxidation of fatty acids by inducing hepatic lipophagy and CPT1α expression (26,27). We thus examined carnitine palmitoyltransferase Iβ (CPT1β) protein expression and found that it was lower in SM of *SM-TRα1*$^{L400R/+}$ mice

(Supplementary Fig. 5A(1)). The expression of CPT1β in muscle from *TRα1*$^{PV/+}$ mice showed a similar trend but was not statistically significant (Supplementary Fig. 5B(1)). We next performed transcriptome pathway analyses of SM from *SM-TRα1*$^{L400R/+}$ mice and *Control* mice, and found that lipid catabolism, lipid transport, and cellular response to hormone stimulus were the major down-regulated pathways in *SM-TRα1*$^{L400R/+}$ mice (Supplementary Table 1(1)). Interestingly, pathways involved in collagen formation and SMAD signaling were upregulated (Supplementary Table 2(1)). We next performed metabolomic profiling of acylcarnitines and TCA cycle intermediates in SM from *SM-TRα1*$^{L400R/+}$ mice. There were decreased levels of some, but not all, species of short, long, and very long chain acylcarnitines compared to *Control* littermates (Fig. 6A). The TCA cycle intermediates, citrate, fumarate, and malate also were decreased suggesting there likely was decreased TCA cycle flux (Fig. 6B). These results suggested that fatty acid utilization might have been impaired due to expression of the TRα1 mutation. Finally, we examined the effect of TRα1 mutation on SM fibre type. There was increased MHC-I and unchanged MHC2a protein levels in SM *TRα1*$^{L400R/+}$ mice (Supplemental Fig. 6A(1)). In *TRα1*$^{PV/+}$ mice, MHC-I protein expression remained the same while there was a decrease in MHC2a (Supplemental Fig. 6B(1)). Thus, the ratios of MHC-1/MHC2a were increased in SM from both mouse lines (Supplemental Fig. 6(1)).

Discussion

While there have been studies examining TRα1-specific regulation of gene expression in the liver, small intestine, bone, and heart (28-31), little is known about TRα1-specific regulation of transcription in SM. Additionally, although the roles of TH on the metabolome and autophagy recently have begun to be examined in SM (10,11), the specific role(s) of TRα1 on these processes in SM is not known. In the current study, we addressed these issues by analyzing gastrocnemius muscle tissue obtained from genetically-altered mice that expressed *TRα1*^{L400R} specifically in SM and *TRα1*^{PV} ubiquitously. Both TRα1 mutants had impaired hormone binding

to TH, decreased transcriptional activity, and dominant negative activity on normal TR isoforms expressed in SM (17,18). We found that expression of both TRα1 mutants in SM led to accumulation of p62 as well as decreased expression of lysosomal membrane proteins and proteases (Figs. 1 and 2), suggesting that there was a late block in autophagy. We found evidence for increased mTOR activity as there was increased phosphorylation of mTOR targets, p70S6K, 4EBP1, and TFEB in SM that expressed TRα1 mutants (Fig. 2C and 3). Increased mTOR activity phosphorylates TFEB (32), the master transcriptional regulator of lysosomal protein expression, to prevent nuclear localization and transcription of lysosomal proteins by TFEB (21). Additionally, we found decreased phosphorylation of AMPK and its downstream target, ATGL. The decreased phosphorylation of AMPK may be due to decreased ATP utilization in SM when TH action is inhibited (33) and also would decrease autophagy (34,35). These findings are consistent with our earlier findings that TH stimulated autophagy by activating AMPK and inhibiting mTOR signaling in metabolically active organs such as liver and SM (11,22).

Muscle-specific deletion of the crucial autophagic gene Atg7 caused accumulation of dysfunctional mitochondria (36). Furthermore, deletion of Atg7 in adult mice just prior to exercise led to damaged mitochondria and ROS damage (37). These results indicated that mitophagy had a fundamental role in maintaining muscle function during physical activity. Our previous studies demonstrated TH promoted mitochondrial quality control through mitophagy and mitochondrial biogenesis (22,24). In this connection, we found that mutant TRα1 expression in SM led to decreased levels of Drp1 and Parkin expression (Fig. 4 and Supplementary Fig. 3(1)). Drp1-mediated fission appears to be a crucial prerequisite for mitophagy, and the upregulation of Drp1 is associated with mitophagy during the early differentiation of muscle cells (38), and TH-mediated stimulation of hepatic mitophagy (22,24). Expression of mutant TRα1 in SM also decreased protein levels of PGC1α, TFAM, and ERRα (Fig. 5), key transcription factors involved in mitochondrial biogenesis are regulated by TH (24), as well as decreased mitochondrial protein

levels of TOMM20, VDAC1 and COXIV (Fig. 5). Taken together, these findings suggested that there was decreased mitochondrial biogenesis and mitochondria content.

Hypothyroid patients are more dependent on muscle glycogen due to impaired ability to use fatty acids (39-41). A decrease in the amount of functional mitochondria in SM could lead to altered mitochondrial fuel utilization (42). To address this issue, we performed transcriptome pathway analyses of SM from *SM-TRα1*$^{L400R/+}$ and *Control* mice. Interestingly, *SM-TRα1*$^{L400R/+}$ mice displayed down-regulation of pathways involved in lipid catabolism (Supplementary Table 2(1)). We observed decreased expression of CPT1β (Supplementary Fig. 5A(1)), which imports acylcarnitines into the mitochondria. Our observation that there were decreases in intracellular acylcarnitines combined with decreases in citrate, fumarate, and malate levels in SM from mice expressing *TRα1*^{L400R} further supports the notion that fatty acid utilization was impaired when dominant negative TRα1 was expressed in SM (Fig. 6). Since the levels of long and very long chain acylcarnitine species were decreased, it is possible that the entry of free fatty acids into mitochondria for β-oxidation was impaired in SM expressing *TRα1*^{L400R} due to the reduction in CPT1β expression. Lipolysis of triglycerides from fat droplets and lipophagy are two major ways in which triglycerides are hydrolyzed to release of free fatty acids for β-oxidation by mitochondria. In this connection, we found decreased phosphorylation of ATGL (Fig. 3D and F) accompanied decreased autophagy (Fig. 1). Thus, decreased mitochondrial biogenesis, CPT1β expression, and autophagy shed light on why hypothyroid patients may have impaired fatty acid utilization in SM.

TH regulates SM fiber type to determine fuel utilization by converting slow twitch fibers that utilize fatty acids to fast twitch fibers that use glucose (10,11). TH directly regulates the expression of genes involved in SM contraction and glucose metabolism (43-45). We previously showed that TH increased the transcription of MHC2a and decreased MHC-I protein expression most likely via autophagy (11). Interestingly, we observed both increased MHC-I protein expression and decreased autophagy in SM from *TRα1*$^{L400R/+}$ mice (Supplemental Fig. 6A(1)). In

283 *TRα1*$^{PV/+}$ mice, MHC2a protein expression was decreased whereas MHC-I remained the same
284 (Supplemental Fig. 6B(1)); thus, the ratio of MHC1/MHC2a protein expression increased in both
285 mouse strains. Currently, the precise molecular mechanism(s) determining SM fiber type
286 expression in *SM-TRα1*$^{L400R/+}$ and *TRα1*$^{PV/+}$ mice remains unclear. Moreover, it is not known
287 whether the aberrant fiber type switching is a consequence of decreased local or systemic TH
288 action. Nonetheless, our findings suggest that expression of slow twitch MHC-1 muscle fibers
289 were favored over fast twitch MHC2a fibers in the SM of both mouse models. Similarly, it was
290 reported that MHCI expression increased and MHC2a expression decreased in SM of
291 hypothyroid patients (33). In this connection, TRα KO mice were reported to have decreased
292 strength compared to wild type mice (46). Moreover, *Dio2* KO mice, which have impaired
293 conversion of T_4 to T_3, exhibited decreased strength and endurance as T_3 concentration in SM
294 was reduced by 33% (47). However, another group found that *Dio2* KO mice had a markedly
295 different phenotype than hypothyroid mice as they had a high rate of SM twitch contraction and
296 resistance to fatigue due to down-regulation of PGC1α causing increased conversion to MHC2a
297 muscle fiber type (48). The reason for the differences in findings between these two groups is
298 not known since the KO mice were derived from the original parental line. The exercise behavior
299 and lean mass in *SM-TRα1*$^{L400R/+}$ mice recently were reported by Nicolaisen et al (49). The time
300 to exhaustion on treadmill and lean mass (measured by magnetic resonance imaging) were
301 unchanged in *SM-TRα1*$^{L400R/+}$ mice compared with the littermate controls. Currently, we do not
302 know the reason(s) *SM-TRα1*$^{L400R/+}$ mice maintained normal endurance running capacities. Since
303 young adult animals were used in Nicolaisen's study, it is possible that the development of
304 myopathy may occur when these mice become older. Additionally, TH mediates the muscle fiber
305 switch from slow twitch to fast twitch muscle fibers in soleus muscle (10,11); thus, strength and
306 sprinting would be affected more than endurance running. Performing studies in older mice or
307 testing for skeletal muscle functions mediated by fast twitch muscles could be helpful in
308 assessing the effects of the dominant negative mutant TRα on muscle function.

In summary, we showed that expression of dominant-negative TRα1 mutations in SM in two different mouse models resulted in decreased autophagy, mitochondrial turnover, fatty acid utilization, and TCA cycle flux, as well as altered muscle fiber phenotype. These results provide novel insight into the molecular and metabolic mechanism(s) of TRα1 that underlie the SM changes in energy metabolism observed in hypothyroid patients and individuals with RTHα syndrome.

Author contributions

Conceptualization – J.Z. R.A.S., and P.M.Y.;

Methodology –J.Z., K.G., S.C.,and P.M.Y.;

Investigation –J.Z., K.G., J.P.H., A.L., X.Z., and C.R.H.;

Writing (Original Draft) – J.Z.; P.M.Y;

Writing (Review & Editing) – J.Z., K.G., S.C., and P.M.Y.;

Funding Acquisition –J.Z., K.G., S.C., and P.M.Y.,

Resources –K.G., S.C., and P.M.Y.;

Supervision – P.M.Y.

Funding information

This work was supported by Ministry of Health, A*STAR and National Medical Research Council Singapore grants MOH-000306 (MOH-CSASI19may-0001) and NMRC/CIRG/1457/2016 to PMY; Duke-NUS Medical School and Estate of Tan Sri Khoo Teck Puat Khoo Pilot Award (Collaborative) Duke-NUS-KP (Coll)/2018/0007A to JZ.

Data Availability Statement: Supplementary Figures(1) of Thyroid hormone receptor alpha regulates autophagy, mitochondrial biogenesis, and fatty acid utilization in skeletal muscle. Figshare. Deposited on 29 March 2021. https://figshare.com/s/78918d8bb5a44f1d3f24; DOI: 10.6084/m9.figshare.14331599.

References

1. Zhou J. Thyroid hormone receptor alpha regulates autophagy, mitochondrial biogenesis, and fatty acid utilization in skeletal muscle. Supplementary Material. *Endocrinology*. 2021. https://figshare.com/s/78918d8bb5a44f1d3f24; DOI: 10.6084/m9.figshare.14331599.
2. Canaris GJ, Manowitz NR, Mayor G, Ridgway EC. The Colorado thyroid disease prevalence study. *Arch Intern Med*. 2000;160(4):526-534.
3. Taylor PN, Albrecht D, Scholz A, Gutierrez-Buey G, Lazarus JH, Dayan CM, Okosieme OE. Global epidemiology of hyperthyroidism and hypothyroidism. *Nat Rev Endocrinol*. 2018;14(5):301-316.
4. Argov Z, Renshaw PF, Boden B, Winokur A, Bank WJ. Effects of thyroid hormones on skeletal muscle bioenergetics. In vivo phosphorus-31 magnetic resonance spectroscopy study of humans and rats. *J Clin Invest*. 1988;81(6):1695-1701.
5. Khaleeli AA, Edwards RH. Effect of treatment on skeletal muscle dysfunction in hypothyroidism. *Clin Sci (Lond)*. 1984;66(1):63-68.
6. Bloise FF, Cordeiro A, Ortiga-Carvalho TM. Role of thyroid hormone in skeletal muscle physiology. *J Endocrinol*. 2018;236(1):R57-R68.
7. Milanesi A, Lee JW, Yang A, Liu YY, Sedrakyan S, Cheng SY, Perin L, Brent GA. Thyroid Hormone Receptor Alpha is Essential to Maintain the Satellite Cell Niche During Skeletal Muscle Injury and Sarcopenia of Aging. *Thyroid*. 2017;27(10):1316-1322.
8. Salvatore D, Simonides WS, Dentice M, Zavacki AM, Larsen PR. Thyroid hormones and skeletal muscle--new insights and potential implications. *Nat Rev Endocrinol*. 2014;10(4):206-214.
9. de Lange P, Senese R, Cioffi F, Moreno M, Lombardi A, Silvestri E, Goglia F, Lanni A. Rapid activation by 3,5,3'-L-triiodothyronine of adenosine 5'-monophosphate-activated protein kinase/acetyl-coenzyme a carboxylase and akt/protein kinase B signaling pathways: relation to changes in fuel metabolism and myosin heavy-chain protein content in rat gastrocnemius muscle in vivo. *Endocrinology*. 2008;149(12):6462-6470.
10. Zhou J, Parker DC, White JP, Lim A, Huffman KM, Ho JP, Yen PM, Kraus WE. Thyroid Hormone Status Regulates Skeletal Muscle Response to Chronic Motor Nerve Stimulation. *Front Physiol*. 2019;10:1363.
11. Lesmana R, Sinha RA, Singh BK, Zhou J, Ohba K, Wu Y, Yau WW, Bay BH, Yen PM. Thyroid Hormone Stimulation of Autophagy Is Essential for Mitochondrial Biogenesis and Activity in Skeletal Muscle. *Endocrinology*. 2016;157(1):23-38.
12. Yen PM. Physiological and molecular basis of thyroid hormone action. *Physiol Rev*. 2001;81(3):1097-1142.
13. Mullur R, Liu YY, Brent GA. Thyroid hormone regulation of metabolism. *Physiol Rev*. 2014;94(2):355-382.
14. Bochukova E, Schoenmakers N, Agostini M, Schoenmakers E, Rajanayagam O, Keogh JM, Henning E, Reinemund J, Gevers E, Sarri M, Downes K, Offiah A, Albanese A, Halsall D, Schwabe JW, Bain M, Lindley K, Muntoni F, Vargha-Khadem F, Dattani M, Farooqi IS, Gurnell M, Chatterjee K. A mutation in the thyroid hormone receptor alpha gene. *N Engl J Med*. 2012;366(3):243-249.
15. van Mullem A, van Heerebeek R, Chrysis D, Visser E, Medici M, Andrikoula M, Tsatsoulis A, Peeters R, Visser TJ. Clinical phenotype and mutant TRalpha1. *N Engl J Med*. 2012;366(15):1451-1453.
16. Moran C, Schoenmakers N, Agostini M, Schoenmakers E, Offiah A, Kydd A, Kahaly G, Mohr-Kahaly S, Rajanayagam O, Lyons G, Wareham N, Halsall D, Dattani M, Hughes S, Gurnell M, Park SM, Chatterjee K. An adult female with resistance to thyroid hormone mediated by defective thyroid hormone receptor alpha. *J Clin Endocrinol Metab*. 2013;98(11):4254-4261.

17. Kaneshige M, Suzuki H, Kaneshige K, Cheng J, Wimbrow H, Barlow C, Willingham MC, Cheng S. A targeted dominant negative mutation of the thyroid hormone alpha 1 receptor causes increased mortality, infertility, and dwarfism in mice. *Proc Natl Acad Sci U S A*. 2001;98(26):15095-15100.
18. Quignodon L, Vincent S, Winter H, Samarut J, Flamant F. A point mutation in the activation function 2 domain of thyroid hormone receptor alpha1 expressed after CRE-mediated recombination partially recapitulates hypothyroidism. *Mol Endocrinol*. 2007;21(10):2350-2360.
19. Bassett JH, Boyde A, Zikmund T, Evans H, Croucher PI, Zhu X, Park JW, Cheng SY, Williams GR. Thyroid hormone receptor alpha mutation causes a severe and thyroxine-resistant skeletal dysplasia in female mice. *Endocrinology*. 2014;155(9):3699-3712.
20. Bjorkoy G, Lamark T, Pankiv S, Overvatn A, Brech A, Johansen T. Monitoring autophagic degradation of p62/SQSTM1. *Methods Enzymol*. 2009;452:181-197.
21. Napolitano G, Esposito A, Choi H, Matarese M, Benedetti V, Di Malta C, Monfregola J, Medina DL, Lippincott-Schwartz J, Ballabio A. mTOR-dependent phosphorylation controls TFEB nuclear export. *Nat Commun*. 2018;9(1):3312.
22. Sinha RA, Singh BK, Zhou J, Wu Y, Farah BL, Ohba K, Lesmana R, Gooding J, Bay BH, Yen PM. Thyroid hormone induction of mitochondrial activity is coupled to mitophagy via ROS-AMPK-ULK1 signaling. *Autophagy*. 2015;11(8):1341-1357.
23. Kim SJ, Tang T, Abbott M, Viscarra JA, Wang Y, Sul HS. AMPK Phosphorylates Desnutrin/ATGL and Hormone-Sensitive Lipase To Regulate Lipolysis and Fatty Acid Oxidation within Adipose Tissue. *Mol Cell Biol*. 2016;36(14):1961-1976.
24. Singh BK, Sinha RA, Tripathi M, Mendoza A, Ohba K, Sy JAC, Xie SY, Zhou J, Ho JP, Chang CY, Wu Y, Giguere V, Bay BH, Vanacker JM, Ghosh S, Gauthier K, Hollenberg AN, McDonnell DP, Yen PM. Thyroid hormone receptor and ERRalpha coordinately regulate mitochondrial fission, mitophagy, biogenesis, and function. *Sci Signal*. 2018;11(536).
25. Zhang Y, Xu H. Translational regulation of mitochondrial biogenesis. *Biochem Soc Trans*. 2016;44(6):1717-1724.
26. Sinha RA, You SH, Zhou J, Siddique MM, Bay BH, Zhu X, Privalsky ML, Cheng SY, Stevens RD, Summers SA, Newgard CB, Lazar MA, Yen PM. Thyroid hormone stimulates hepatic lipid catabolism via activation of autophagy. *The Journal of clinical investigation*. 2012;122(7):2428-2438.
27. Zhou J, Waskowicz LR, Lim A, Liao XH, Lian B, Masamune H, Refetoff S, Tran B, Koeberl DD, Yen PM. A Liver-Specific Thyromimetic, VK2809, Decreases Hepatosteatosis in Glycogen Storage Disease Type Ia. *Thyroid*. 2019;29(8):1158-1167.
28. Yen PM, Feng X, Flamant F, Chen Y, Walker RL, Weiss RE, Chassande O, Samarut J, Refetoff S, Meltzer PS. Effects of ligand and thyroid hormone receptor isoforms on hepatic gene expression profiles of thyroid hormone receptor knockout mice. *EMBO Rep*. 2003;4(6):581-587.
29. Kress E, Rezza A, Nadjar J, Samarut J, Plateroti M. The frizzled-related sFRP2 gene is a target of thyroid hormone receptor alpha1 and activates beta-catenin signaling in mouse intestine. *The Journal of biological chemistry*. 2009;284(2):1234-1241.
30. Freudenthal B, Shetty S, Butterfield NC, Logan JG, Han CR, Zhu X, Astapova I, Hollenberg AN, Cheng SY, Bassett JHD, Williams GR. Genetic and Pharmacological Targeting of Transcriptional Repression in Resistance to Thyroid Hormone Alpha. *Thyroid*. 2019;29(5):726-734.
31. Hones GS, Rakov H, Logan J, Liao XH, Werbenko E, Pollard AS, Praestholm SM, Siersbaek MS, Rijntjes E, Gassen J, Latteyer S, Engels K, Strucksberg KH, Kleinbongard P, Zwanziger D, Rozman J, Gailus-Durner V, Fuchs H, Hrabe de Angelis M, Klein-Hitpass L, Kohrle J, Armstrong DL, Grontved L, Bassett JHD, Williams GR, Refetoff S, Fuhrer D, Moeller LC. Noncanonical thyroid hormone signaling mediates cardiometabolic effects in vivo. *Proceedings of the National Academy of Sciences of the United States of America*. 2017;114(52):E11323-E11332.

32. Settembre C, Zoncu R, Medina DL, Vetrini F, Erdin S, Erdin S, Huynh T, Ferron M, Karsenty G, Vellard MC, Facchinetti V, Sabatini DM, Ballabio A. A lysosome-to-nucleus signalling mechanism senses and regulates the lysosome via mTOR and TFEB. *The EMBO journal*. 2012;31(5):1095-1108.
33. Wiles CM, Young A, Jones DA, Edwards RH. Muscle relaxation rate, fibre-type composition and energy turnover in hyper- and hypo-thyroid patients. *Clin Sci (Lond)*. 1979;57(4):375-384.
34. Gwinn DM, Shackelford DB, Egan DF, Mihaylova MM, Mery A, Vasquez DS, Turk BE, Shaw RJ. AMPK phosphorylation of raptor mediates a metabolic checkpoint. *Mol Cell*. 2008;30(2):214-226.
35. Inoki K, Zhu T, Guan KL. TSC2 mediates cellular energy response to control cell growth and survival. *Cell*. 2003;115(5):577-590.
36. Masiero E, Agatea L, Mammucari C, Blaauw B, Loro E, Komatsu M, Metzger D, Reggiani C, Schiaffino S, Sandri M. Autophagy is required to maintain muscle mass. *Cell Metab*. 2009;10(6):507-515.
37. Lo Verso F, Carnio S, Vainshtein A, Sandri M. Autophagy is not required to sustain exercise and PRKAA1/AMPK activity but is important to prevent mitochondrial damage during physical activity. *Autophagy*. 2014;10(11):1883-1894.
38. Sin J, Andres AM, Taylor DJ, Weston T, Hiraumi Y, Stotland A, Kim BJ, Huang C, Doran KS, Gottlieb RA. Mitophagy is required for mitochondrial biogenesis and myogenic differentiation of C2C12 myoblasts. *Autophagy*. 2016;12(2):369-380.
39. Baldwin KM, Hooker AM, Herrick RE, Schrader LF. Respiratory capacity and glycogen depletion in thyroid-deficient muscle. *J Appl Physiol Respir Environ Exerc Physiol*. 1980;49(1):102-106.
40. McAllister RM, Delp MD, Laughlin MH. Thyroid status and exercise tolerance. Cardiovascular and metabolic considerations. *Sports Med*. 1995;20(3):189-198.
41. Zurcher RM, Horber FF, Grunig BE, Frey FJ. Effect of thyroid dysfunction on thigh muscle efficiency. *J Clin Endocrinol Metab*. 1989;69(5):1082-1086.
42. Muoio DM. Metabolic inflexibility: when mitochondrial indecision leads to metabolic gridlock. *Cell*. 2014;159(6):1253-1262.
43. Ambrosio R, De Stefano MA, Di Girolamo D, Salvatore D. Thyroid hormone signaling and deiodinase actions in muscle stem/progenitor cells. *Mol Cell Endocrinol*. 2017;459:79-83.
44. Desvergne B, Petty KJ, Nikodem VM. Functional characterization and receptor binding studies of the malic enzyme thyroid hormone response element. *J Biol Chem*. 1991;266(2):1008-1013.
45. Weinstein SP, O'Boyle E, Haber RS. Thyroid hormone increases basal and insulin-stimulated glucose transport in skeletal muscle. The role of GLUT4 glucose transporter expression. *Diabetes*. 1994;43(10):1185-1189.
46. Johansson C, Lannergren J, Lunde PK, Vennstrom B, Thoren P, Westerblad H. Isometric force and endurance in soleus muscle of thyroid hormone receptor-alpha(1)- or -beta-deficient mice. *Am J Physiol Regul Integr Comp Physiol*. 2000;278(3):R598-603.
47. Barez-Lopez S, Bosch-Garcia D, Gomez-Andres D, Pulido-Valdeolivas I, Montero-Pedrazuela A, Obregon MJ, Guadano-Ferraz A. Abnormal motor phenotype at adult stages in mice lacking type 2 deiodinase. *PLoS One*. 2014;9(8):e103857.
48. Carmody C, Ogawa-Wong AN, Martin C, Luongo C, Zuidwijk M, Sager B, Petersen T, Roginski Guetter A, Janssen R, Wu EY, Bogaards S, Neumann NM, Hau K, Marsili A, Boelen A, Silva JE, Dentice M, Salvatore D, Wagers AJ, Larsen PR, Simonides WS, Zavacki AM. A Global Loss of Dio2 Leads to Unexpected Changes in Function and Fiber Types of Slow Skeletal Muscle in Male Mice. *Endocrinology*. 2019;160(5):1205-1222.
49. Nicolaisen TS, Klein AB, Dmytriyeva O, Lund J, Ingerslev LR, Fritzen AM, Carl CS, Lundsgaard AM, Frost M, Ma T, Schjerling P, Gerhart-Hines Z, Flamant F, Gauthier K, Larsen S, Richter EA, Kiens B,

Clemmensen C. Thyroid hormone receptor alpha in skeletal muscle is essential for T3-mediated increase in energy expenditure. *FASEB J*. 2020;34(11):15480-15491.

Figure legends

Figure 1. Mutant TRα1 expression impaired autophagic degradation. (A) Immunoblot and densitometric analysis showing protein levels of p62 and LC3B-II in gastrocnemius muscle from *Control* (n=4) and *SM-TRα1*$^{L400R/+}$ (n=4) mice. (B) Immunoblot and densitometric analysis showing protein levels of p62 and LC3B-II in gastrocnemius muscle from *wild-type* (n=5) and *TRα1*$^{PV/+}$ (n=5) mice. Data are shown as mean±SD.

Figure 2. Mutant TRα1 expression decreased levels of lysosomal markers. (A-C) Immunoblot and densitometric analysis showing protein levels of lysosomal markers LAMP1 and LAMP2 (A), lysosomal protease cathepsin D and cathepsin B (B), and phosphorylation of TFEB (C) in gastrocnemius muscle from *Control* (n=4) and *SM-TRα1*$^{L400R/+}$ (n=4) mice. (D) Immunoblot and densitometric analysis showing protein levels of LAMP1, LAMP2, cathepsin D, and cathepsin B in gastrocnemius muscle from *wild-type* (n=5) and *TRα1*$^{PV/+}$ (n=5) mice. (E) Immunoblot and densitometric analysis showing phosphorylation of TFEB in gastrocnemius muscle from *wild-type* (n=5) and *TRα1*$^{PV/+}$ (n=5) mice. Data are shown as mean±SD.

Figure 3. *TRα1*$^{L400R/+}$ expression increased mTOR signaling and decreased AMPK signaling. (A-C) Immunoblot (A) and densitometric analysis (B-C) showing phosphorylation of mTOR targets p70S6 kinase and 4EBP1 and in gastrocnemius muscle from *Control* (n=4) and *SM-TRα1*$^{L400R/+}$ (n=4) mice. (D-F) Immunoblot (D) and densitometric analysis (E-F) showing phosphorylation AMPK and ATGL in gastrocnemius muscle from *Control* (n=4) and *SM-TRα1*$^{L400R/+}$ (n=4) mice. Data are shown as mean±SD.

Figure 4. *TRα1*$^{L400R/+}$ expression decreased protein levels of Drp1 and parkin. (A-D) Immunoblot (A) and densitometric analysis (B-D) showing protein levels of factors for mitochondrial quality

control, Drp1, parkin and PINK in gastrocnemius muscle from *Control* (n=4) and *SM-TRα1*$^{L400R/+}$ (n=4) mice. Data are shown as mean±SD.

Figure 5. Mutant TRα1 expression impaired mitochondrial biogenesis. (A-C) Immunoblot and densitometric analysis showing protein levels of key regulators for mitochondrial biogenesis, PGC1α, TFAM, and ERRα (A), mitochondrial proteins TOMM20 and VDAC1 (B), and COXIV (C) in gastrocnemius muscle from *Control* (n=4) and *SM-TRα1*$^{L400R/+}$ (n=4) mice. (D) Immunoblot and densitometric analysis showing levels of PGC1α, TFAM, ERRα, TOMM20, VDAC1, and COXIV in gastrocnemius muscle from *wild-type* (n=5) and *TRα1*$^{PV/+}$ (n=5) mice. Data are shown as mean±SD.

Figure 6. Mutant TRα1 expression impaired fatty acid and TCA cycle metabolism. The levels of acylcarnitines (A) and organic acids (B) in gastrocnemius muscle from *Control* (n=4) and *SM-TRα1*$^{L400R/+}$ (n=3) mice. Data are shown as mean±SD.

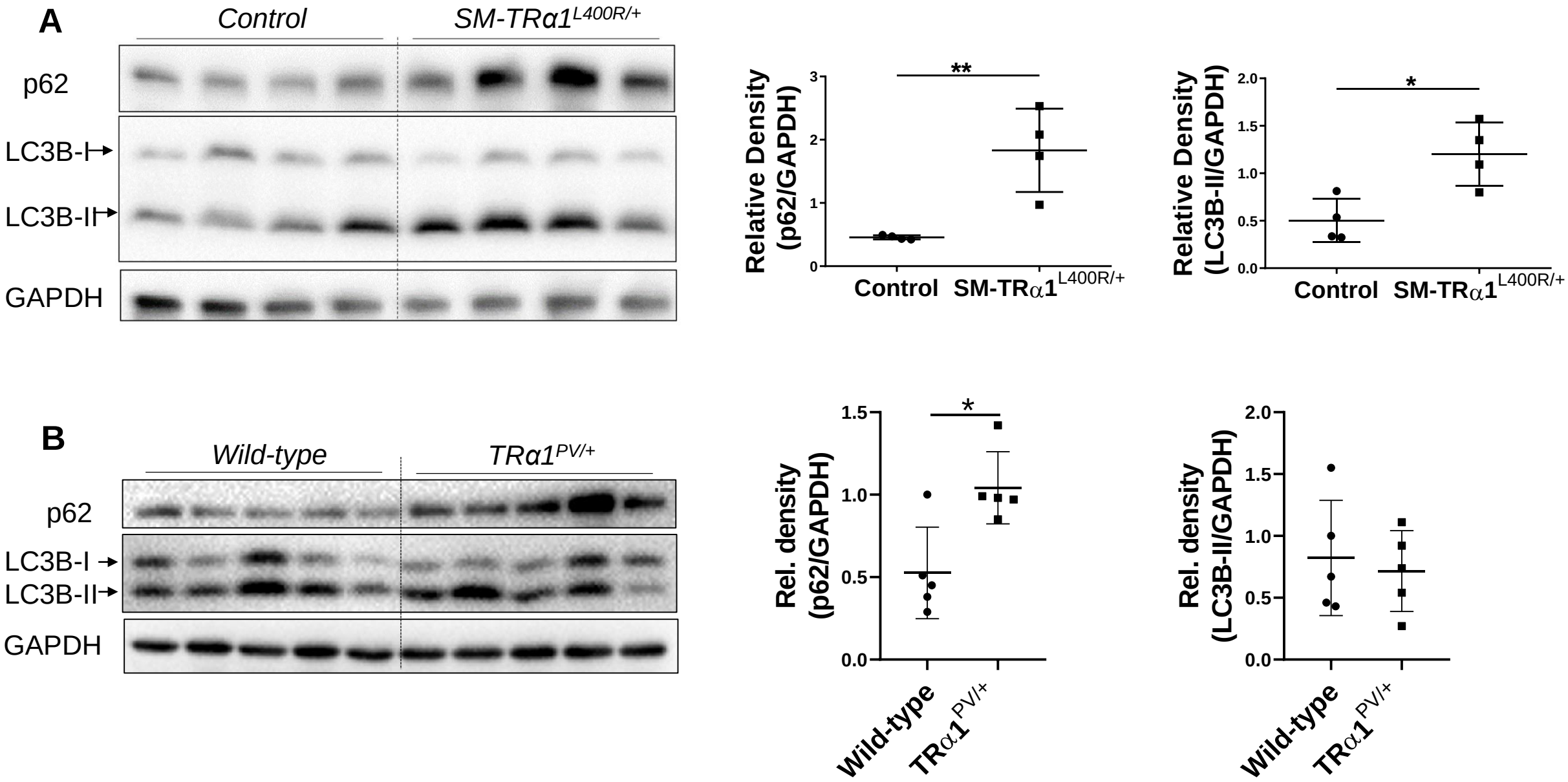
A
Control
SM-TRα1L400R/+
p62
LC3B-I
LC3B-II
GAPDH
Relative Density (p62/GAPDH)
**
Control
SM-TRα1L400R/+
Relative Density (LC3B-II/GAPDH)
*
Control
SM-TRα1L400R/+
B
Wild-type
TRα1PV/+
p62
LC3B-I
LC3B-II
GAPDH
Rel. density (p62/GAPDH)
*
Wild-type
TRα1PV/+
Rel. density (LC3B-II/GAPDH)
Wild-type
TRα1PV/+

Figure 1

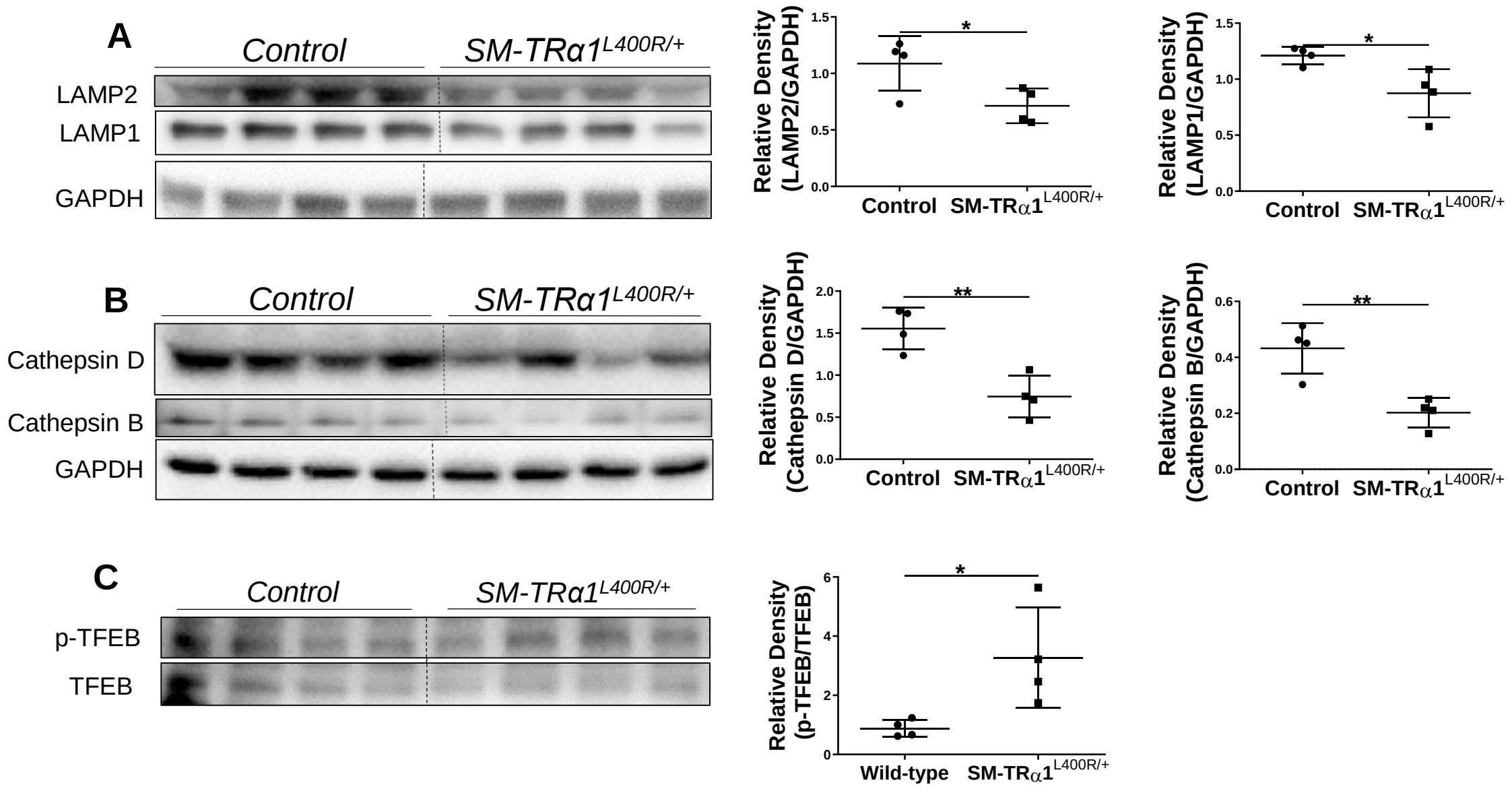
A
Control
SM-TRα1L400R/+
LAMP2
LAMP1
GAPDH
Relative Density (LAMP2/GAPDH)
Relative Density (LAMP1/GAPDH)
Control
SM-TRα1L400R/+
B
Cathepsin D
Cathepsin B
Relative Density (Cathepsin D/GAPDH)
Relative Density (Cathepsin B/GAPDH)
C
p-TFEB
TFEB
Relative Density (p-TFEB/TFEB)
Wild-type

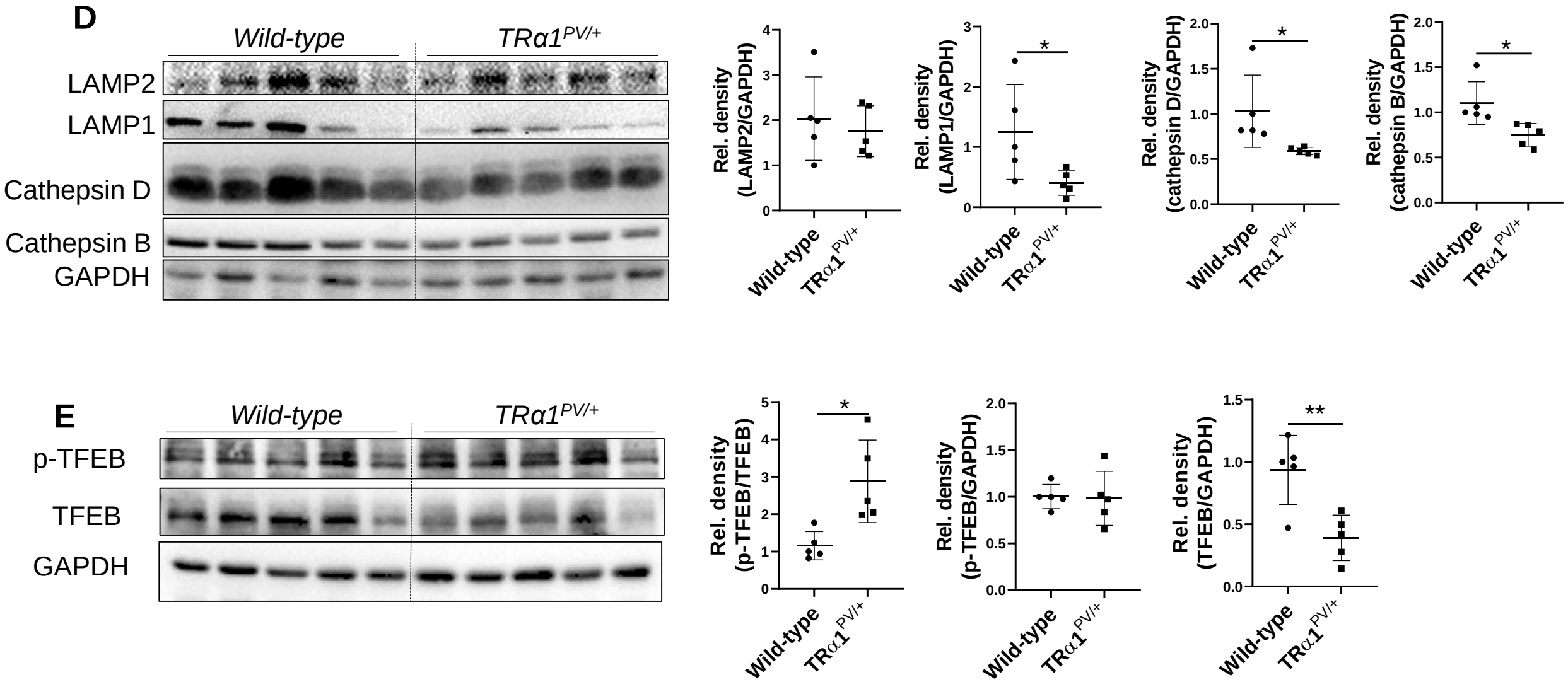
D
Wild-type
TRα1PV/+
LAMP2
LAMP1
Cathepsin D
Cathepsin B
GAPDH
Rel. density (LAMP2/GAPDH)
Rel. density (LAMP1/GAPDH)
Rel. density (cathepsin D/GAPDH)
Rel. density (cathepsin B/GAPDH)
Wild-type
TRα1PV/+
E
Wild-type
TRα1PV/+
p-TFEB
TFEB
GAPDH
Rel. density (p-TFEB/TFEB)
Rel. density (p-TFEB/GAPDH)
Rel. density (TFEB/GAPDH)
Wild-type
TRα1PV/+

Figure 2

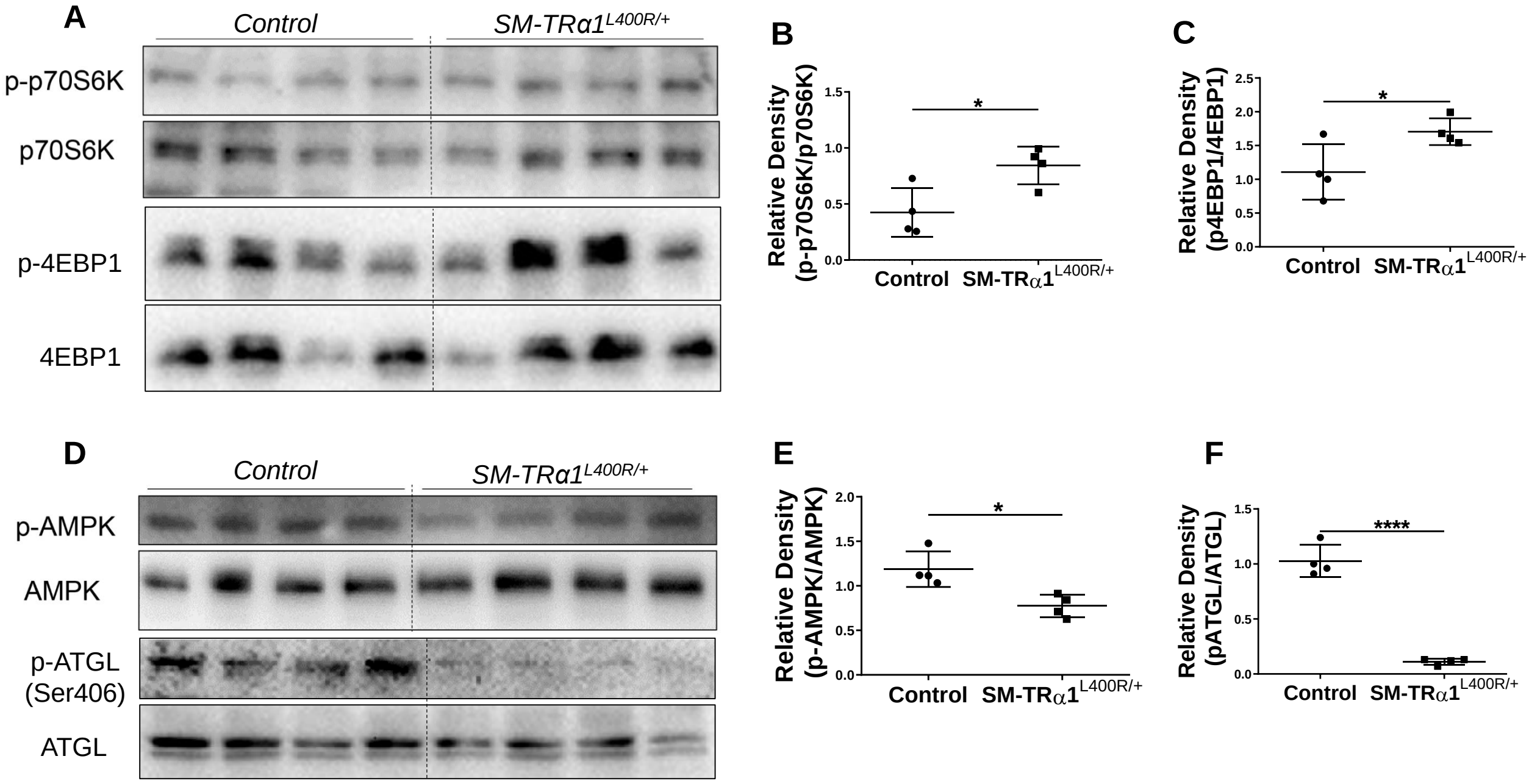
A
Control
SM-TRα1L400R/+
p-p70S6K
p70S6K
p-4EBP1
4EBP1
B
Relative Density
(p-p70S6K/p70S6K)
1.5
1.0
0.5
0.0
*
Control
SM-TRα1L400R/+
C
Relative Density
(p4EBP1/4EBP1)
2.5
2.0
1.5
1.0
0.5
0.0
*
Control
SM-TRα1L400R/+
D
Control
SM-TRα1L400R/+
p-AMPK
AMPK
p-ATGL
(Ser406)
ATGL
E
Relative Density
(p-AMPK/AMPK)
2.0
1.5
1.0
0.5
0.0
*
Control
SM-TRα1L400R/+
F
Relative Density
(pATGL/ATGL)
1.5
1.0
0.5
0.0
****
Control
SM-TRα1L400R/+

Figure 3

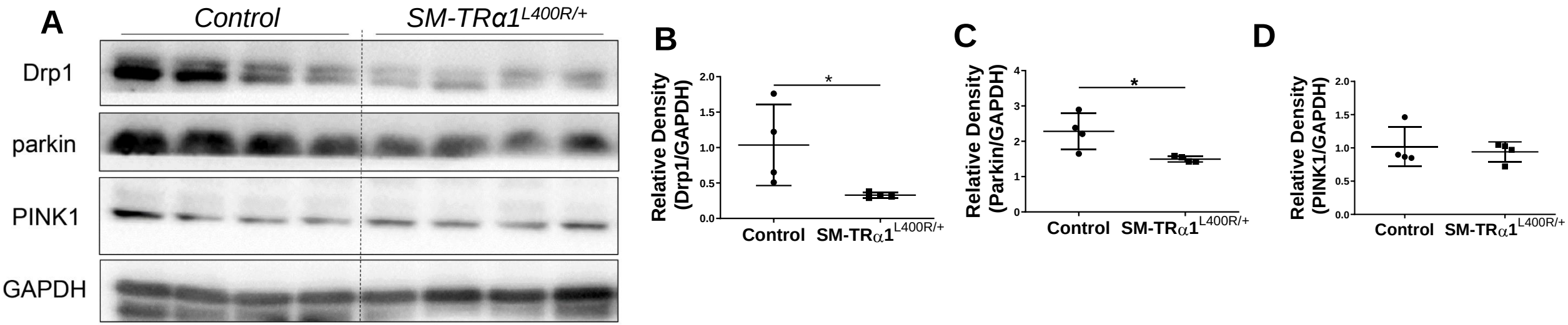
A
Control
SM-TRα1L400R/+
Drp1
parkin
PINK1
GAPDH
B
Relative Density (Drp1/GAPDH)
2.0
1.5
1.0
0.5
0.0
*
Control
SM-TRα1L400R/+
C
Relative Density (Parkin/GAPDH)
4
3
2
1
0
*
Control
SM-TRα1L400R/+
D
Relative Density (PINK1/GAPDH)
2.0
1.5
1.0
0.5
0.0
Control
SM-TRα1L400R/+

Figure 4

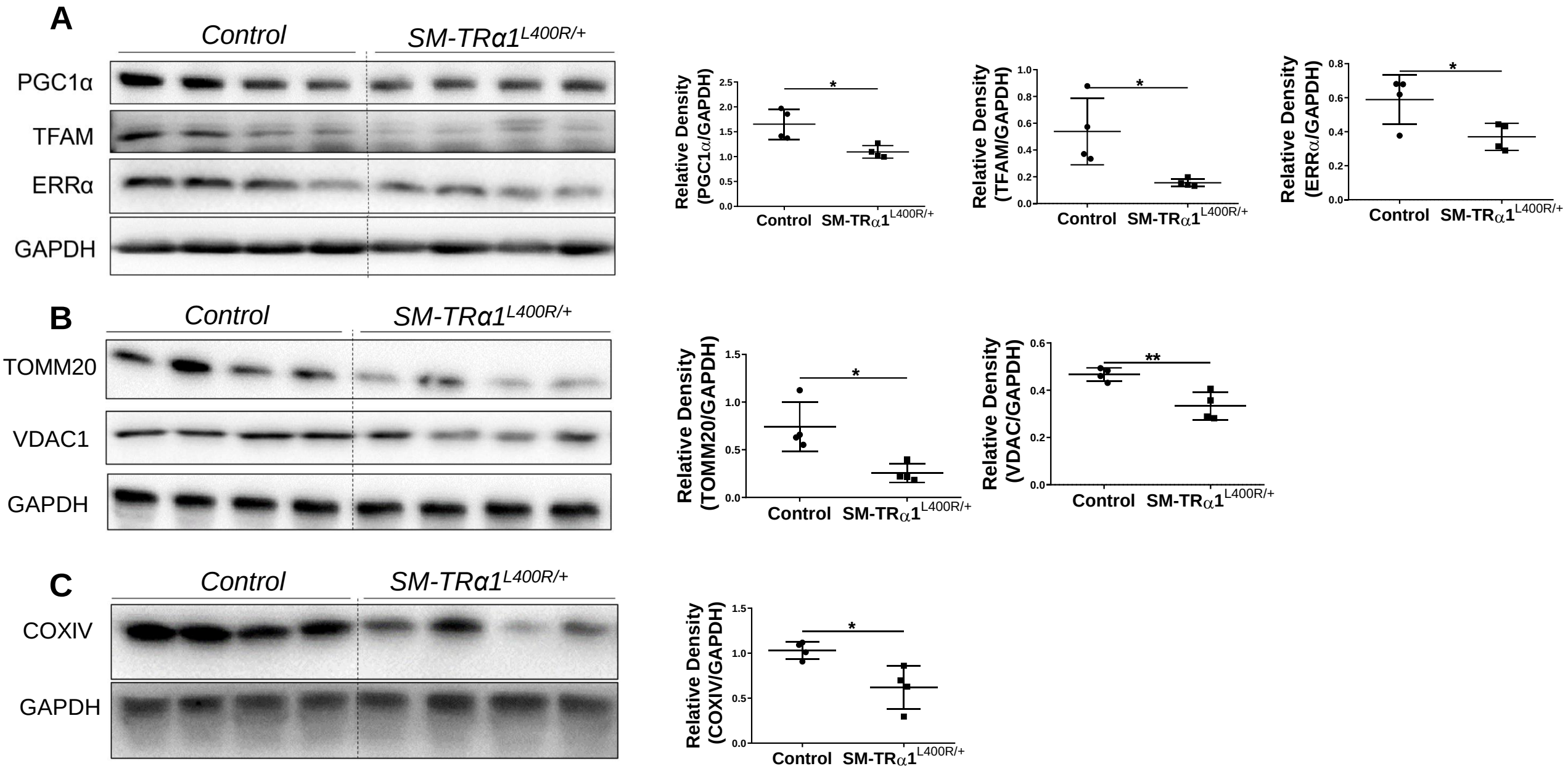
A
Control
SM-TRα1L400R/+
PGC1α
TFAM
ERRα
GAPDH
Relative Density (PGC1α/GAPDH)
Relative Density (TFAM/GAPDH)
Relative Density (ERRα/GAPDH)
Control
SM-TRα1L400R/+
B
TOMM20
VDAC1
GAPDH
Relative Density (TOMM20/GAPDH)
Relative Density (VDAC/GAPDH)
C
COXIV
GAPDH
Relative Density (COXIV/GAPDH)

D

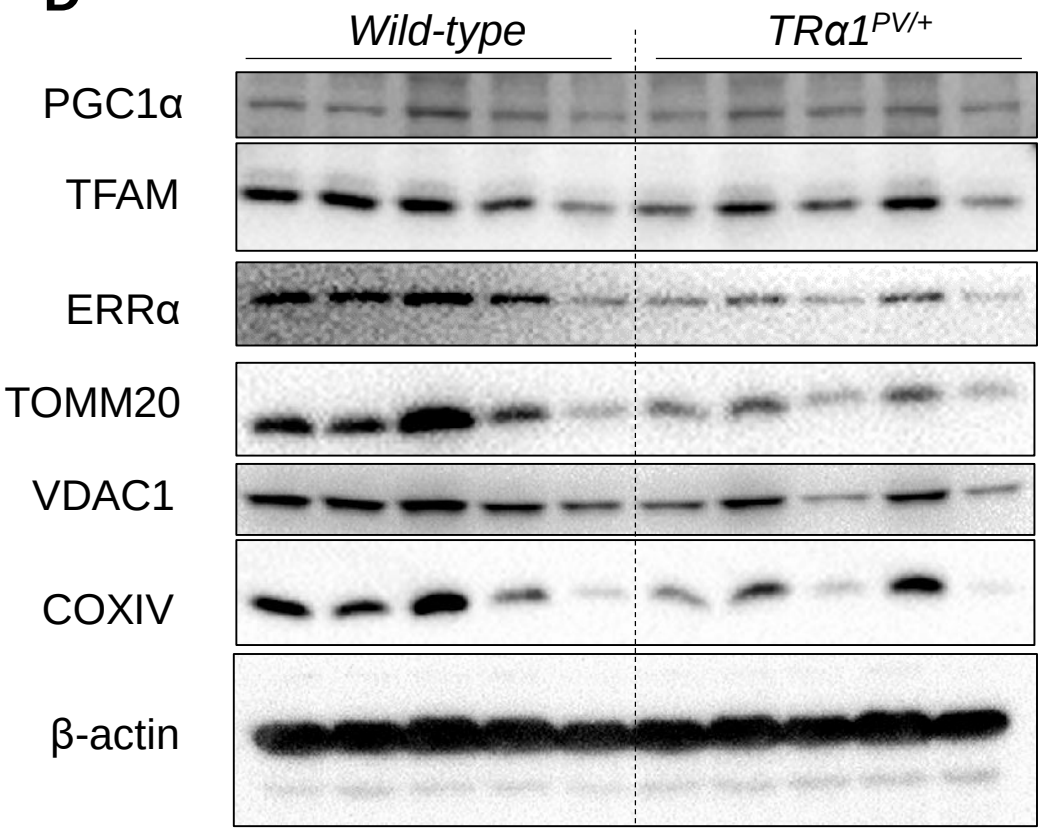
Wild-type
TRα1PV/+
PGC1α
TFAM
ERRα
TOMM20
VDAC1
COXIV
β-actin

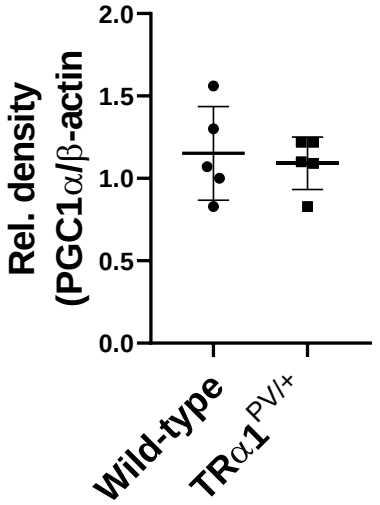
Rel. density (PGC1α/β-actin)
2.0
1.5
1.0
0.5
0.0
Wild-type
TRα1PV/+

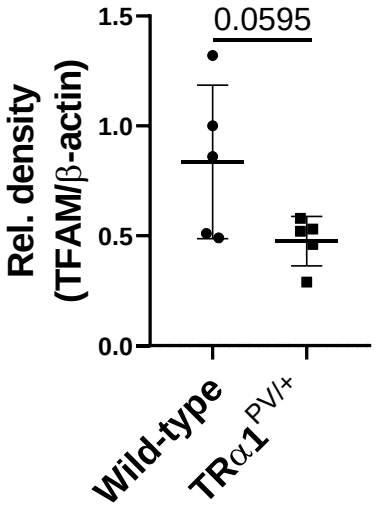
Rel. density (TFAM/β-actin)
0.0595
1.5
1.0
0.5
0.0
Wild-type
TRα1PV/+

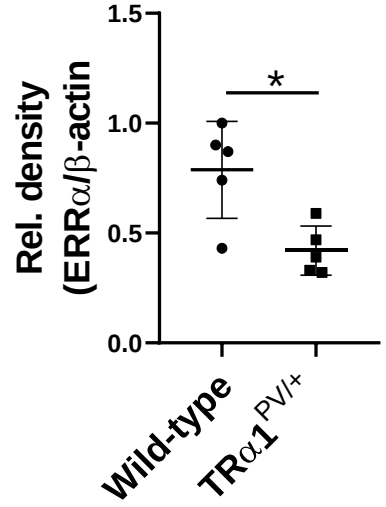
Rel. density (ERRα/β-actin
*
1.5
1.0
0.5
0.0
Wild-type
TRα1PV/+

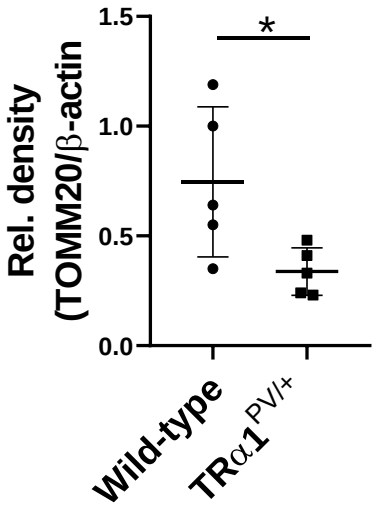
Rel. density (TOMM20/β-actin
*
1.5
1.0
0.5
0.0
Wild-type
TRα1PV/+

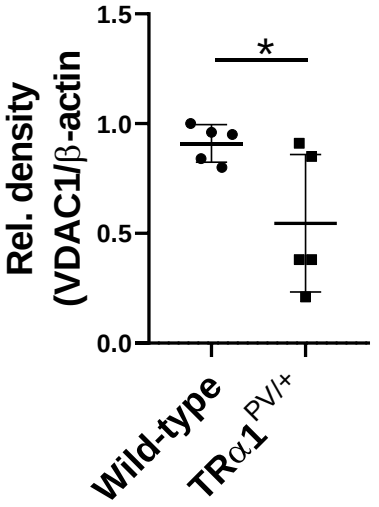
Rel. density (VDAC1/β-actin
*
1.5
1.0
0.5
0.0
Wild-type
TRα1PV/+

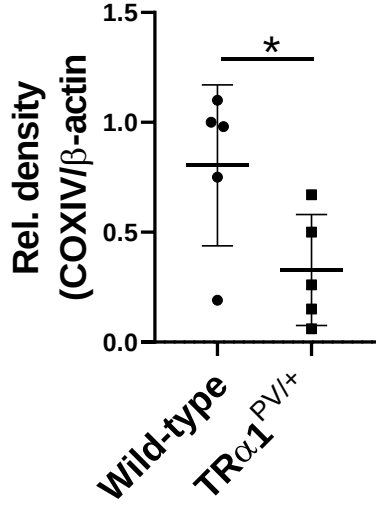
Rel. density (COXIV/β-actin
*
1.5
1.0
0.5
0.0
Wild-type
TRα1PV/+

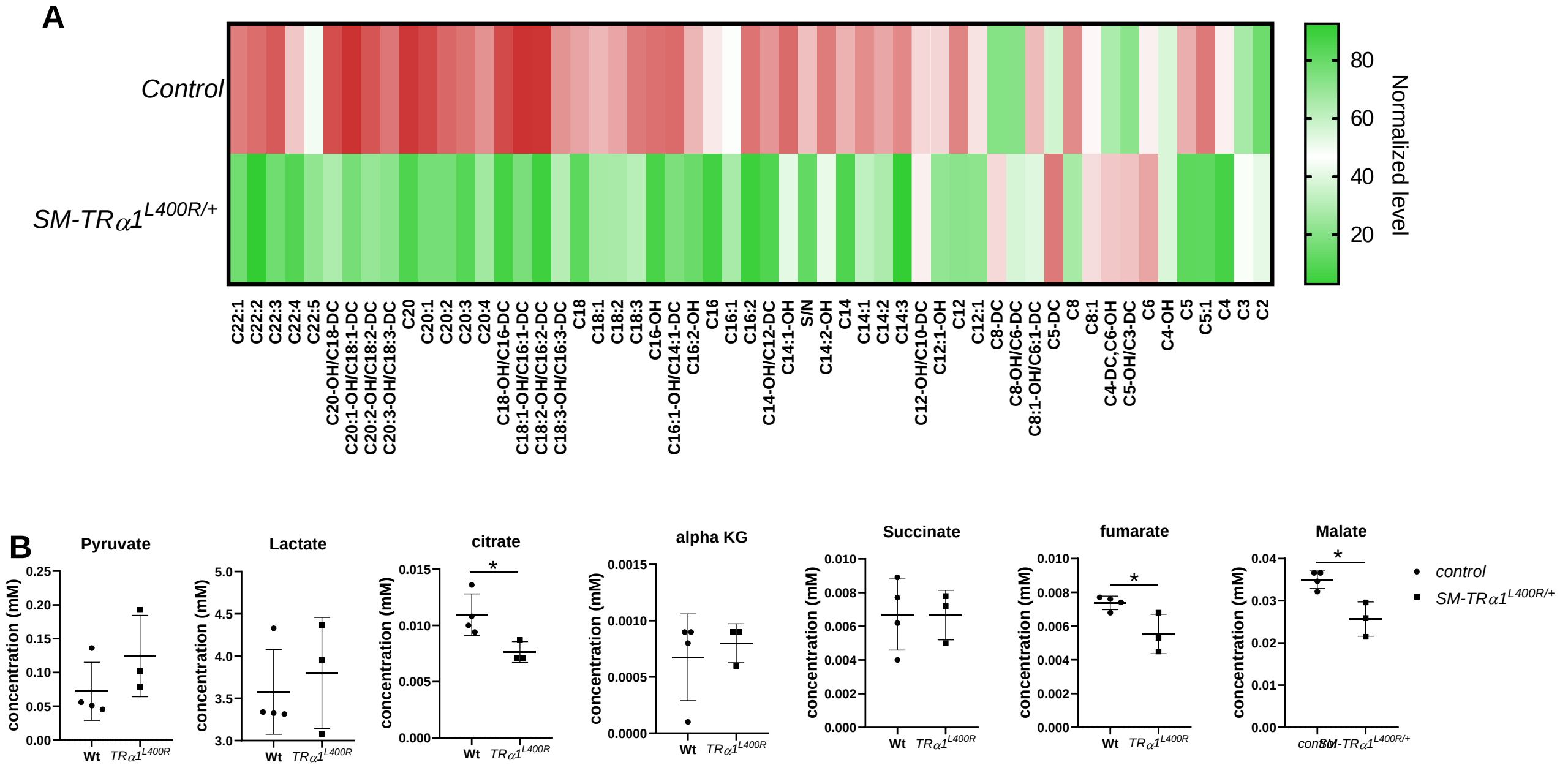
A
Control
SM-TRα1L400R/+
Normalized level
80
60
40
20
C22:1
C22:2
C22:3
C22:4
C22:5
C20-OH/C18-DC
C20:1-OH/C18:1-DC
C20:2-OH/C18:2-DC
C20:3-OH/C18:3-DC
C20
C20:1
C20:2
C20:3
C20:4
C18-OH/C16-DC
C18:1-OH/C16:1-DC
C18:2-OH/C16:2-DC
C18:3-OH/C16:3-DC
C18
C18:1
C18:2
C18:3
C16-OH
C16:1-OH/C14:1-DC
C16:2-OH
C16
C16:1
C16:2
C14-OH/C12-DC
C14:1-OH
S/N
C14:2-OH
C14
C14:1
C14:2
C14:3
C12-OH/C10-DC
C12:1-OH
C12
C12:1
C8-DC
C8-OH/C6-DC
C8:1-OH/C6:1-DC
C5-DC
C8
C8:1
C4-DC,C6-OH
C5-OH/C3-DC
C6
C4-OH
C5
C5:1
C4
C3
C2
B
Pyruvate
Lactate
citrate
alpha KG
Succinate
fumarate
Malate
concentration (mM)
Wt
TRα1L400R
control
SM-TRα1L400R/+
*

Figure 6

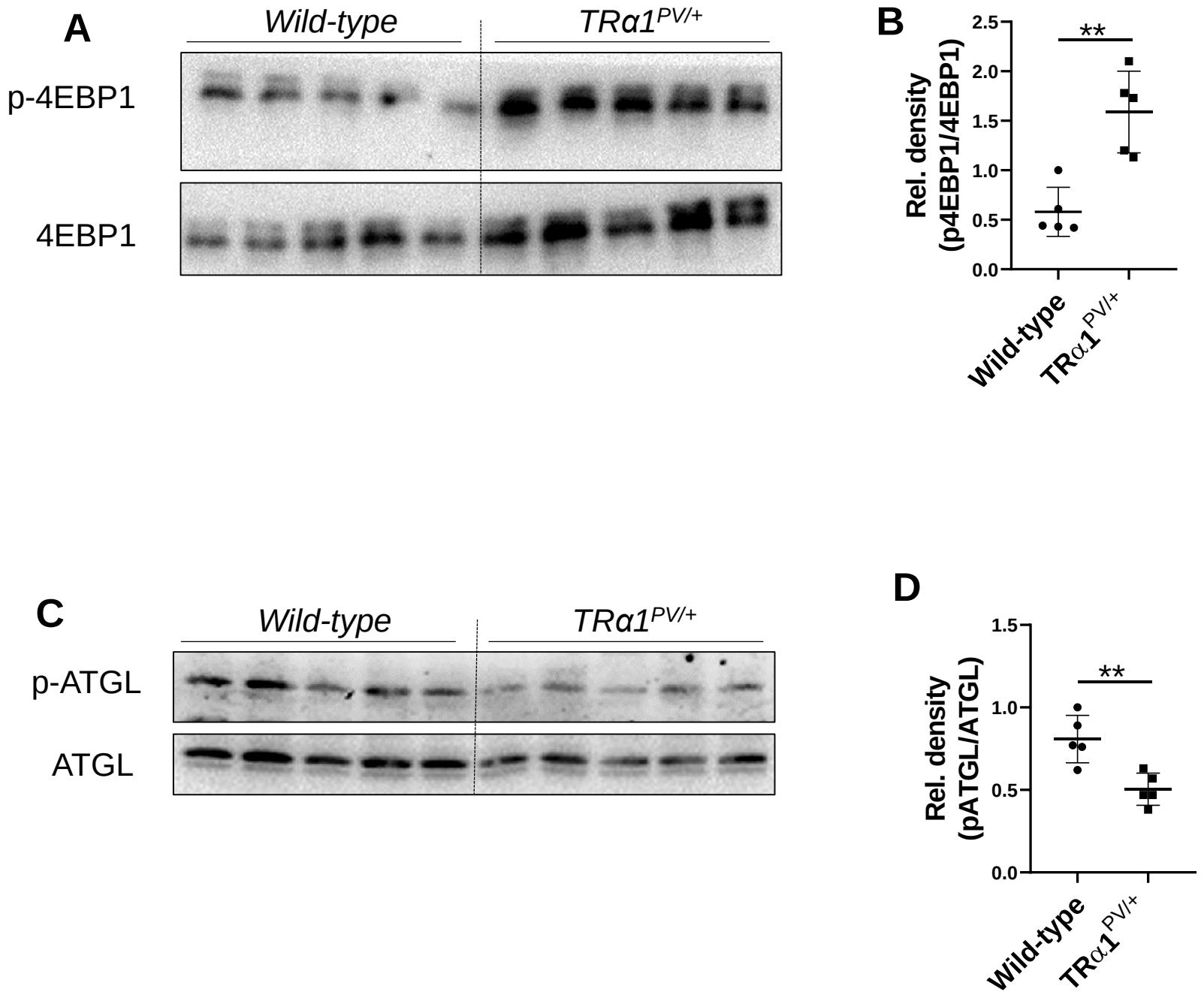

Supplementary Figure 1

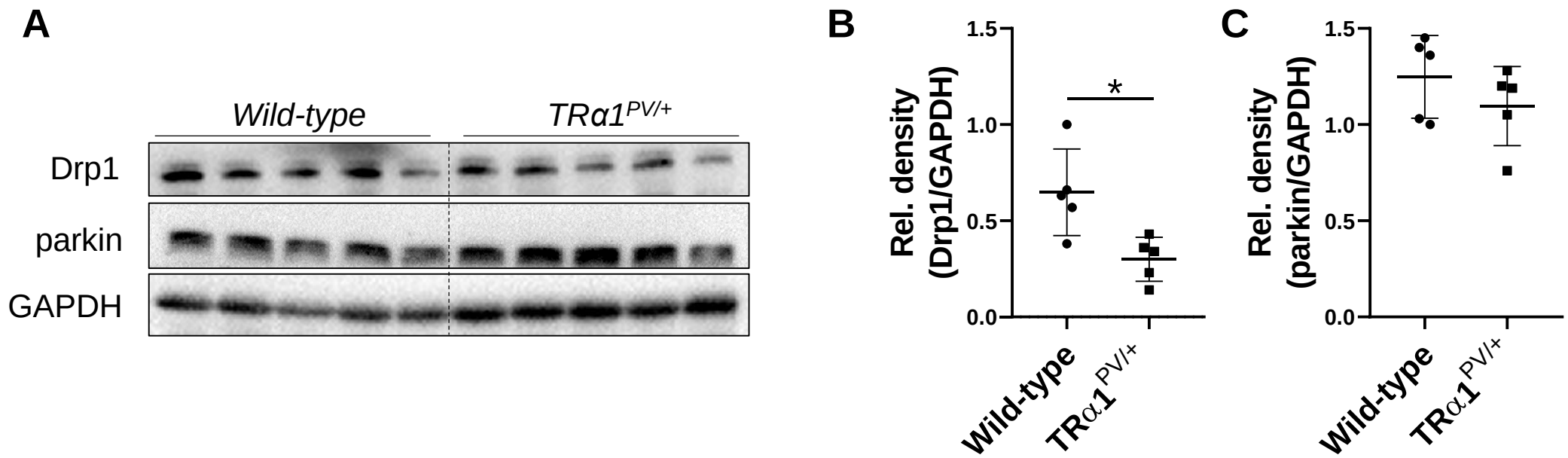

Supplementary Figure 2

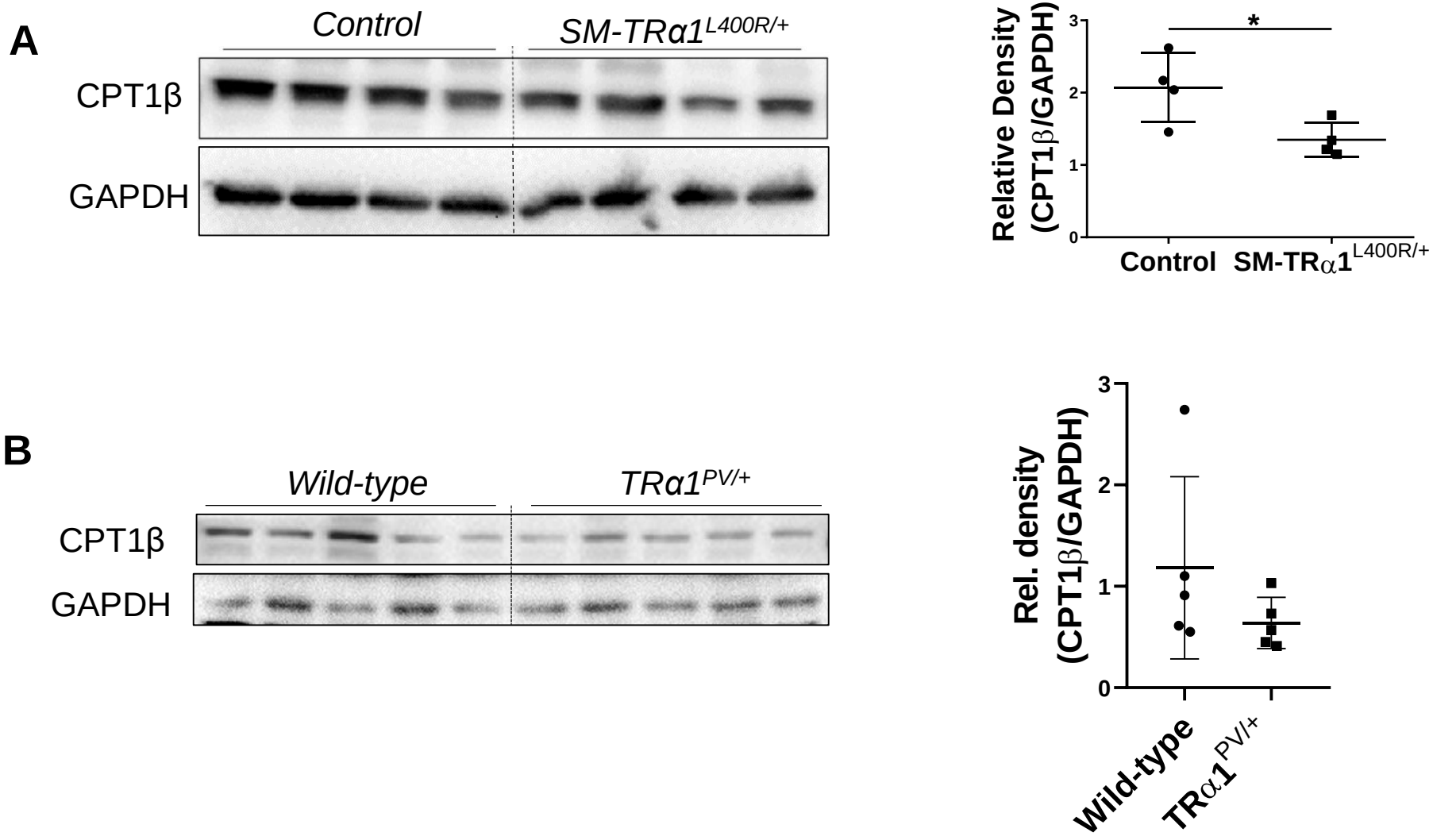

Supplementary Figure 3

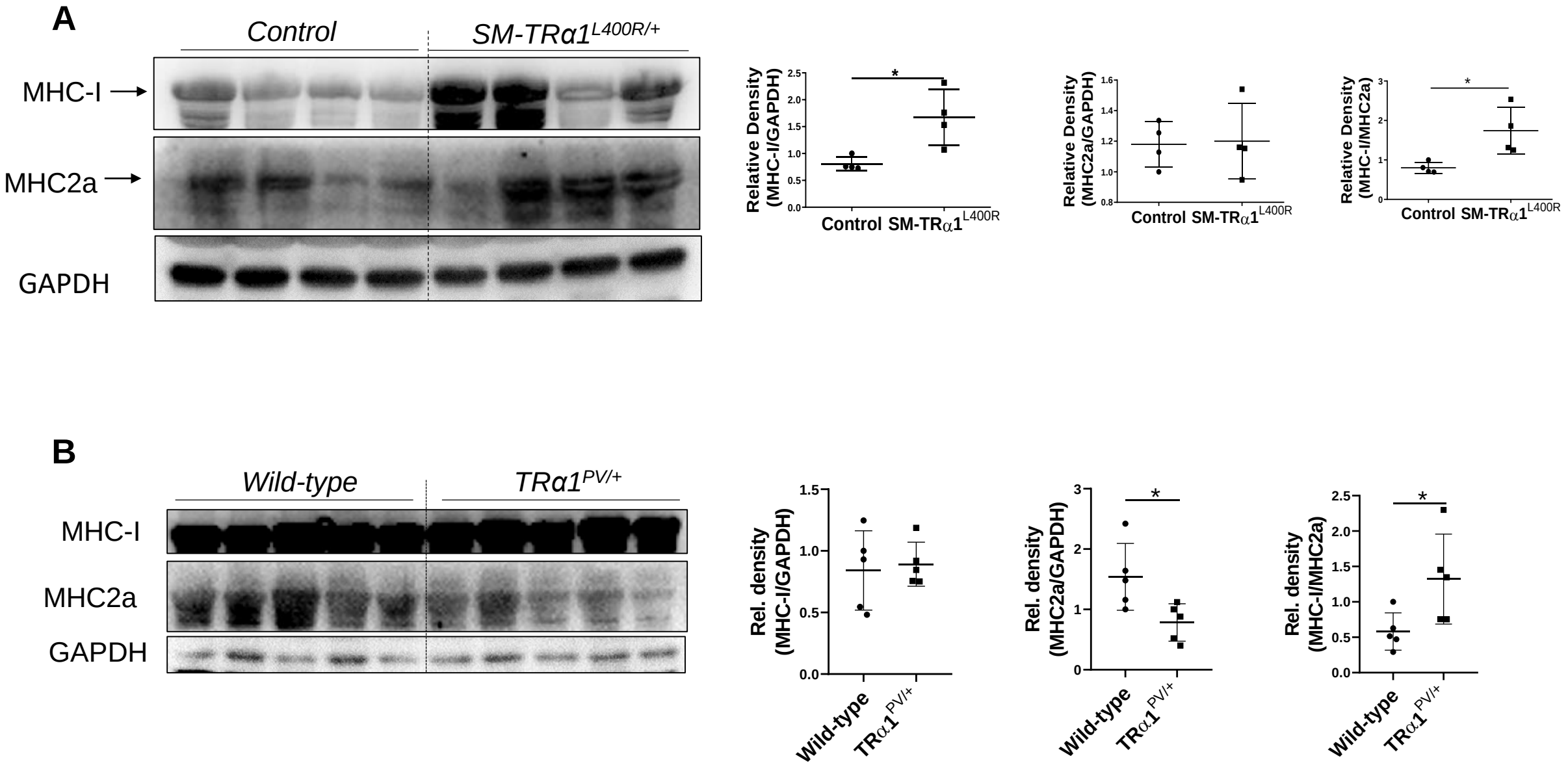

Supplementary Figure 4

Supplementary table 1. Antibody list

Antibody	Company	Catalogue number
LC3B	Cell Signaling Technology	2775
p62		5114
AMPK		5831
p-AMPK (Thr172)		2535
p-P70S6K (Thr389)		9205
P70S6K		9202
4EBP1		9452
p-4EBP1 (Thr37/46)		2855
Tomm20		42406
COXIV		4850
Drp1		8570
parkin		4211
LAMP1		9091
GAPDH		5174
VDAC1		4661

Antibody	Company	Catalogue number
cathepsin B	Santa Cruz Biotechnology	sc-13985
cathepsin D		sc-6486
β-actin		sc-47778
p-ATGL (Ser406)	Abcam	ab135093
ATGL		ab99532
ERRa		07-662
CPT1β		ab134988
TFAM		ab131607
PINK1		ab23707
TFEB		ab2636
p-TFEB (Ser142)	Millipore	ABE1971
PGC1a	Sigma Chemical Co	SAB2500781
LAMP2	Thermo Fisher Scientific	PA1-655

Supplementary Table 2. Pathway analysis of differentially expressed genes in the gastrocnemius muscle from *SM-TRα1$^{L400R/+}$ vs. Control* mice

SM-TRα1$^{L400R/+}$ vs. Control	**Pathway ID**	**description**	**Adjusted p-value**	**Gene list**
Down-regulated	GO:0046461	neutral lipid catabolic process	0.00074	Apob|Ces1d|Cps1|Apoa2|Apoc3|Apoa1|
	GO:0032870	cellular response to hormone stimulus	0.001445	Aldob|Rhoq|Fgb|Apob|Acvr1|Nr6a1|Fyn|Eif5a|Nr3c1|Arg1|Rxrg|Egr1|Junb|Fos|Cpeb2|Myo5a|Uri1|Mef2c|Plcb1|Cacna1h|Jak2|Tsc1|Akt3|Cps1|
	GO:0032368	regulation of lipid transport	0.012703	Acsl4|Mapk9|Apoa2|Abca7|Pla2g6|Apoa1|Apoc3|Atp8a1|
	GO:0006639	acylglycerol metabolic process	0.001501	Apoa1|G6pc|Agpat1|Apoc3|Cps1|Slc27a5|Acsl4|Apoa2|Apob|Ces1d|
	GO:0032409	regulation of transporter activity	0.013862	Myo5a|Apoa2|Cbarp|Camk2d|Plcb1|Pla2g6|Mef2c|Gpd1l|Neto2|Kmt2a|Cacng7|Wnk2|
Up-regulated	GO:0005581	collagen	8.58E-08	Col4a2|Col5a2|Col11a2|Col11a1|Col1a1|Col5a1|Col5a3|Col15a1|Col6a1|Col6a3|Col12a1|Col3a1|Col4a1|Col14a1|Pcolce|Col19a1|Col6a2|Col1a2|
	GO:0071560	cellular response to transforming growth factor beta stimulus	2.31E-07	Nrep|Peg10|Aspn|Ankrd1|Smad5|Col1a1|Fbn1|Axin1|Smad2|Fn1
	GO:0046332	SMAD binding	1.33E-05	Ankrd1|Flna|Acvr1|Mef2a|Pml|Smad7|Col5a2|Zeb2|Col3a1|Tcf12|Rnf111|Col1a2|Sma

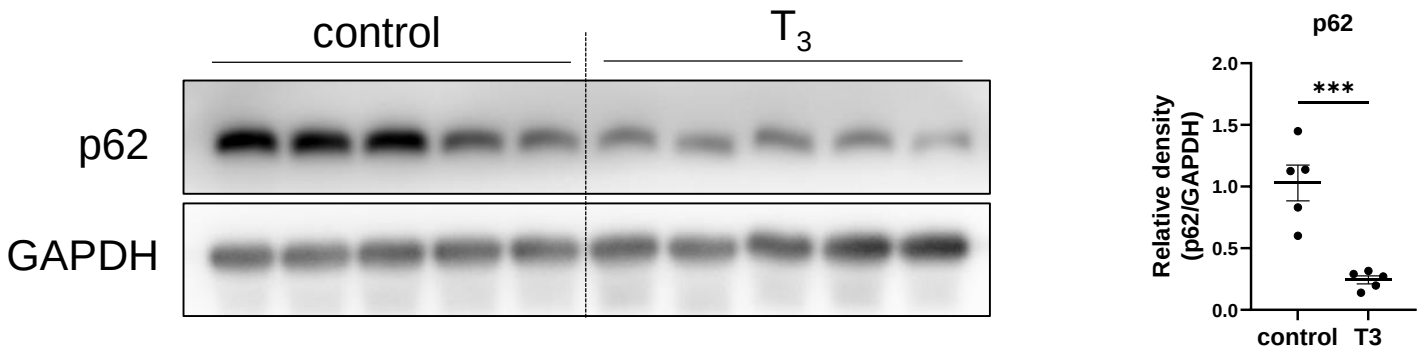

Supplementary Figure 1. T_3 decreased p62 in gastrocnemius muscle. Immunoblot and densitometric analysis of p62 in gastrocnemius muscle from control or T3 injected wildtype male C57BL/6 mice. T_3 was given through intraperitoneal injection at a dose of 20 µg/100g body weight for 10 consecutive days.

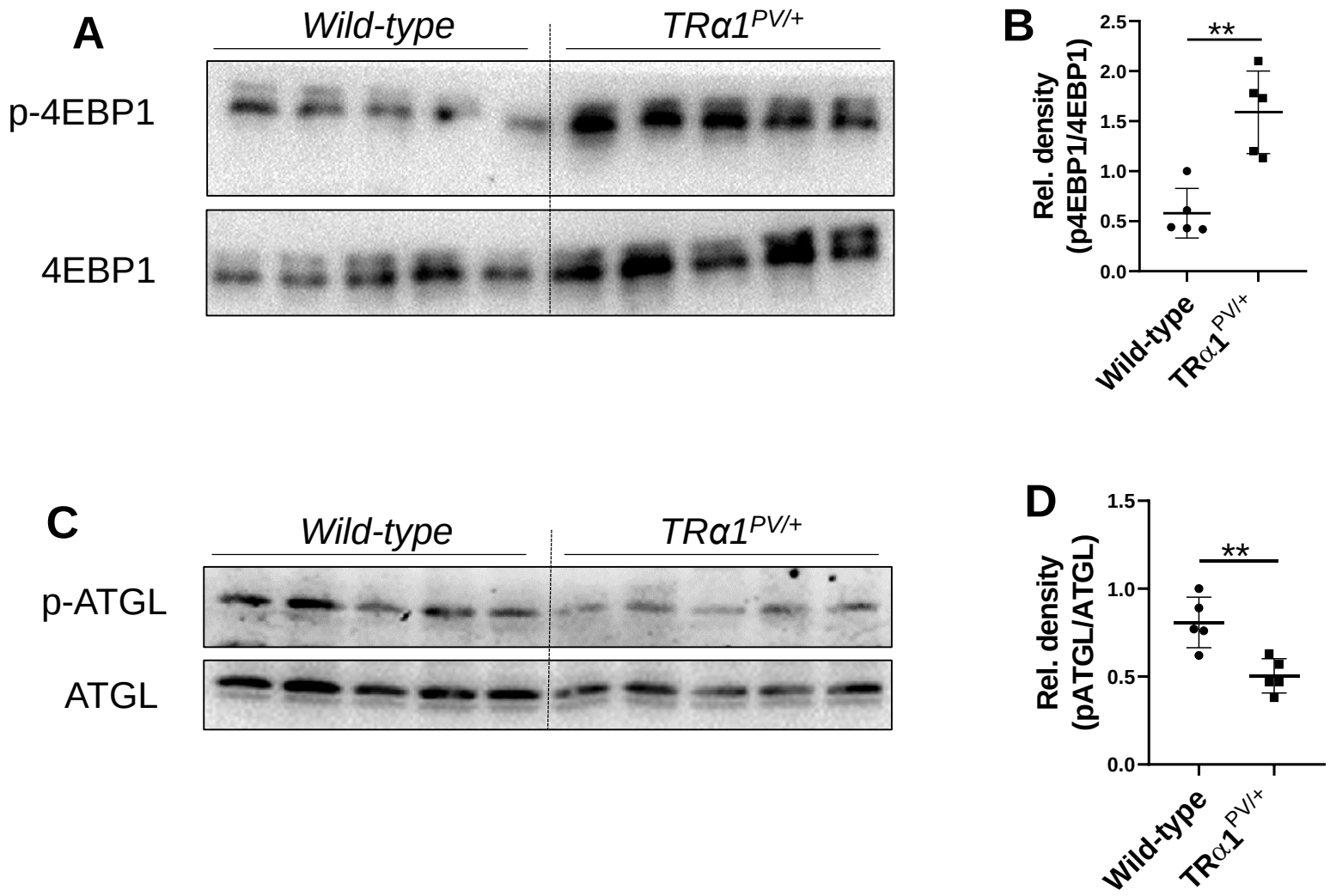

Supplementary Figure 2. *TRα1^{PV}* expression increased phosphorylation of 4EBP1, and decreased phosphorylation of ATGL. (A-B) Immunoblot (A) and densitometric analysis (B) showing phosphorylation of 4EBP1 and 4EBP1 in gastrocnemius muscle from *wild-type* (n=5) and *TRα1$^{PV/+}$* (n=5) mice. (C-D) Immunoblot (C) and densitometric analysis (D) showing phosphorylation ATGL in gastrocnemius muscle from *wild-type* (n=5) and *TRα1$^{PV+/}$* (n=5) mice. Data are shown as mean±SD.

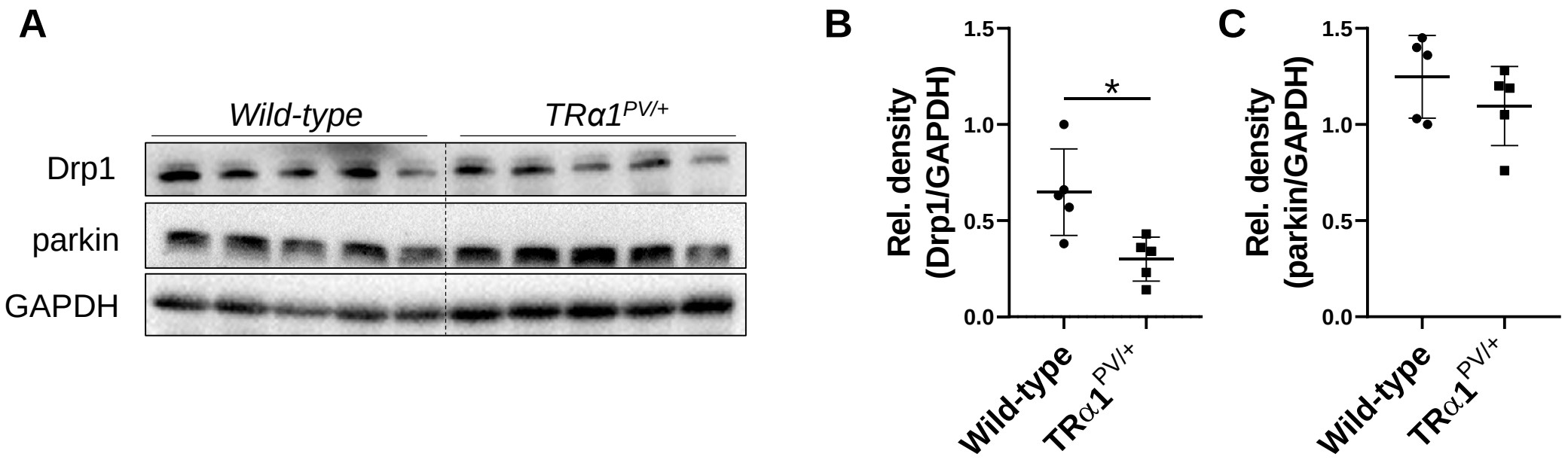

Supplementary Figure 3. TRα1^{PV} expression decreased protein level of Drp1 but not parkin. (A-C) Immunoblot (A) and densitometric analysis (B-C) showing protein level of Drp1 and parkin in gastrocnemius muscle from *wild-type* (n=5) and *TRα1$^{PV/+}$* (n=5) mice. Data are shown as mean±SD.

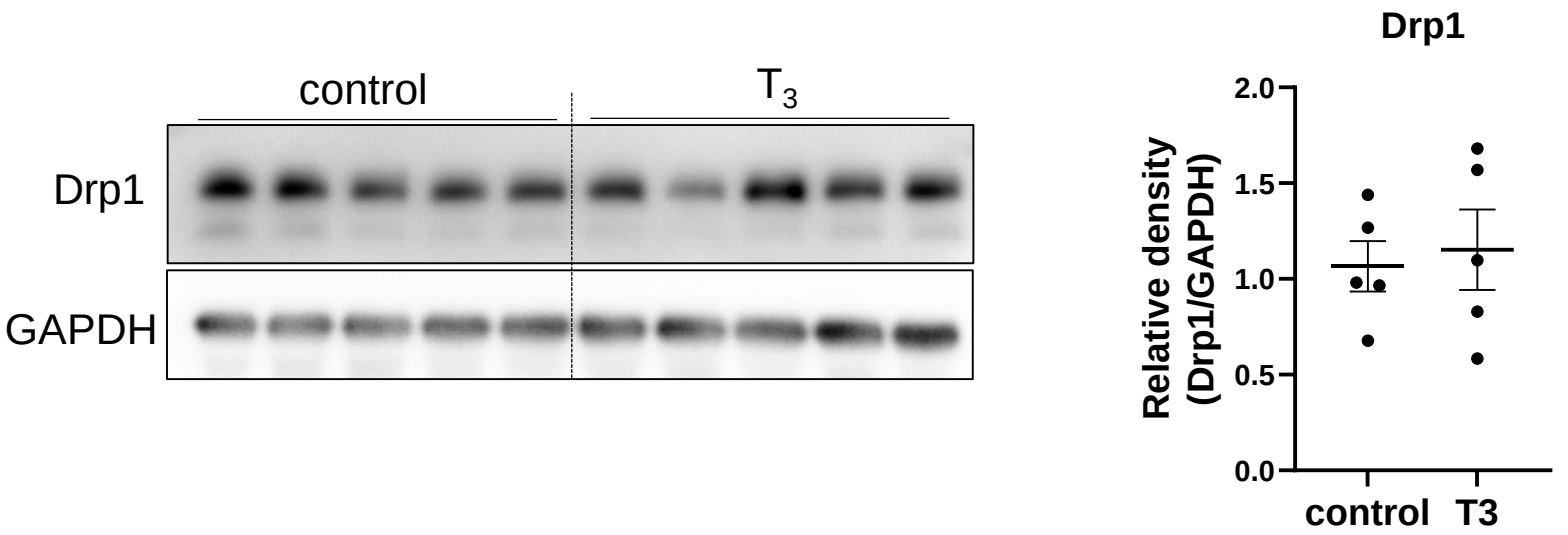

Supplementary Figure 4. T_3 injection didn't affect Drp1 in gastrocnemius muscle from wildtype C57BL/6. Immunoblot and densitometric analysis of Drp1 in gastrocnemius muscle from control or T3 injected wildtype male C57BL/6 mice. T_3 was given through intraperitoneal injection at a dose of 20 µg/100g body weight for 10 consecutive days.

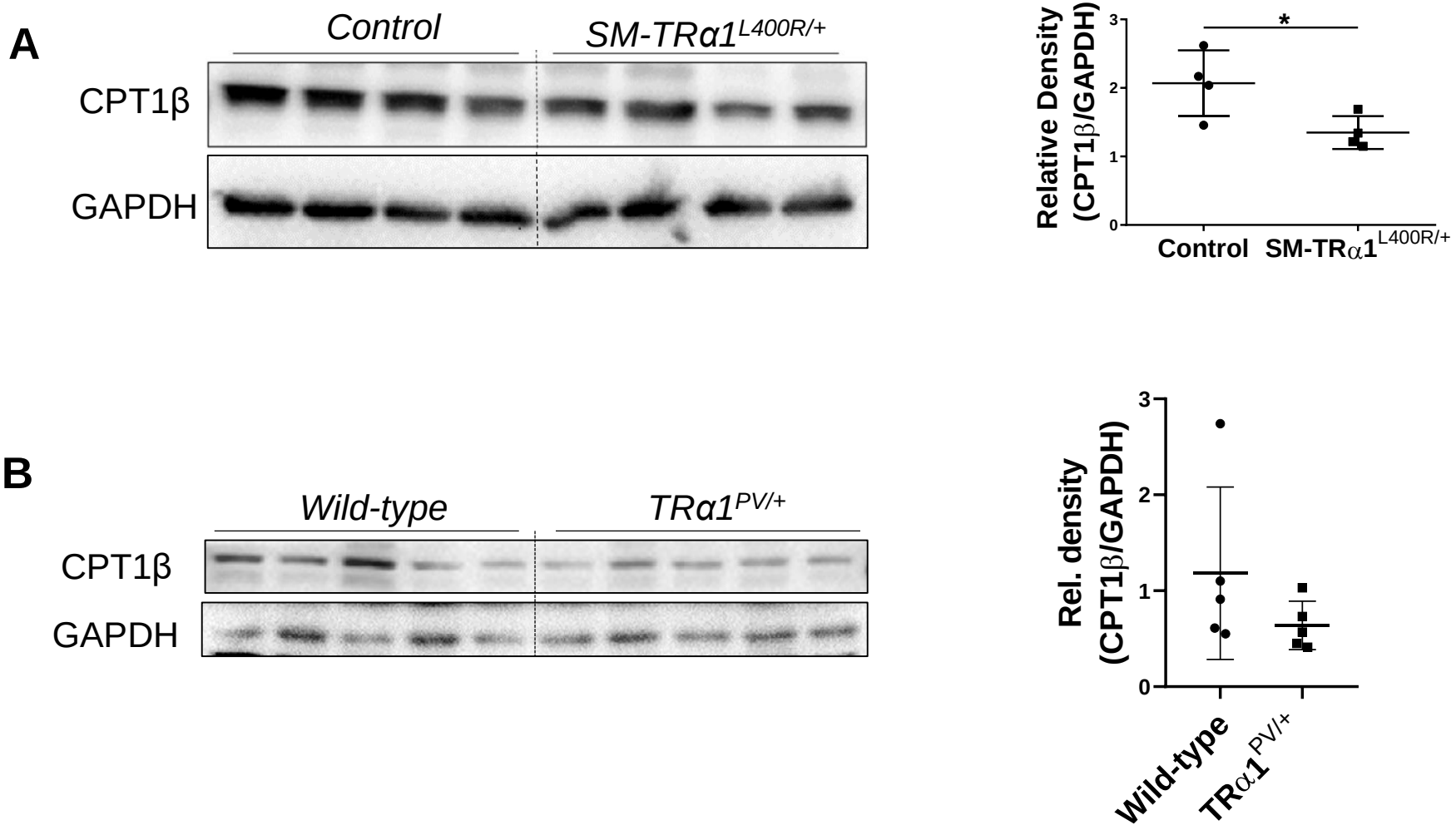

Supplementary Figure 5. The effect of mutant TRα1 expression on protein level of CPT1β. (A) Immunoblot and densitometric analysis showing protein level of CPT1β in gastrocnemius muscle from *Control* (n=4) and *SM-TRα1*$^{L400R/+}$ (n=4) mice. (B) Immunoblot and densitometric analysis showing protein levels of CPT1β in gastrocnemius muscle from *wild-type* (n=5) and *TRα1*$^{PV/+}$ (n=5) mice. Data are shown as mean±SD.

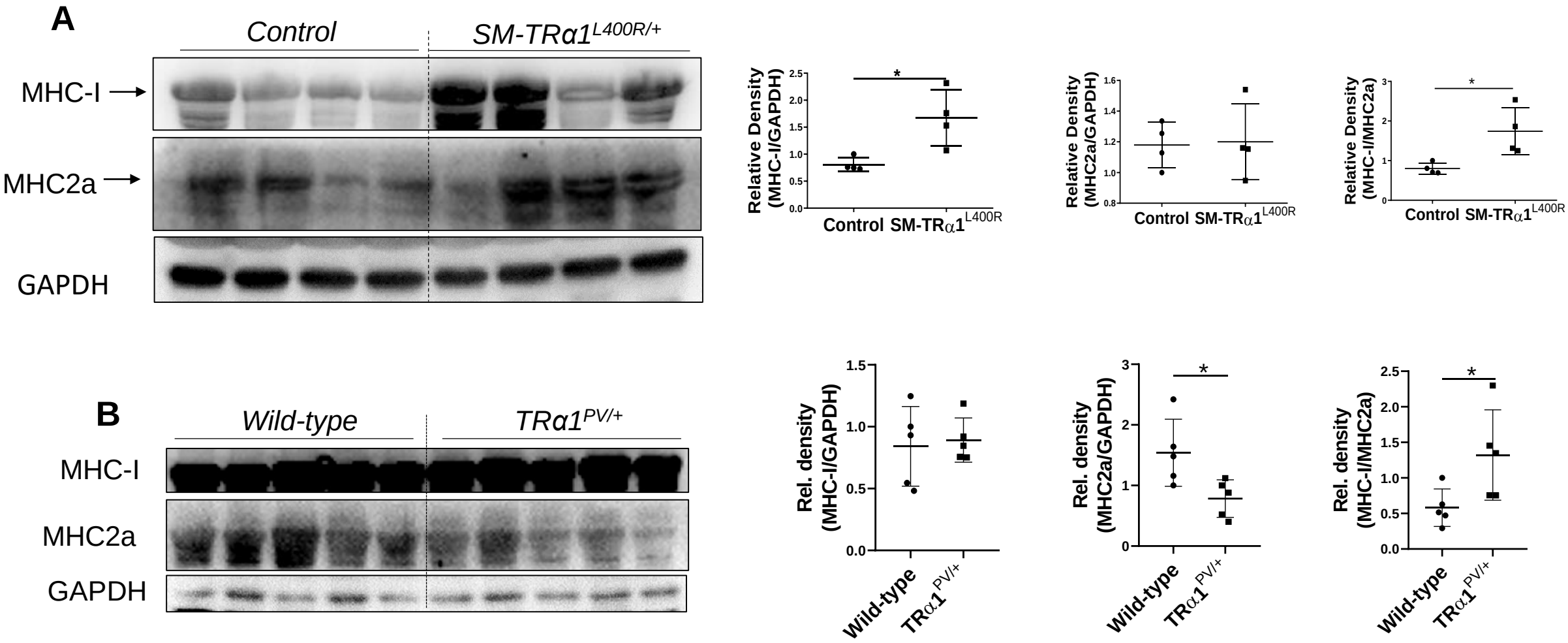

Supplementary Figure 6. Protein levels of MHC-I and MHC2a in gastrocnemius muscle. (A) Immunoblot and densitometric analysis showing protein levels of MHC-I and MHC2a in gastrocnemius muscle from *Control* (n=4) and *SM-TRα1*$^{L400R/+}$ (n=4) mice (A) or wild-type (n=5) and *TRα1*$^{PV/+}$ (n=5) mice (B). Data are shown as mean±SD.

Supplementary table 1. Antibody list

Antibody	Company	Catalogue number
LC3B	Cell Signaling Technology	2775
p62		5114
AMPK		5831
p-AMPK (Thr172)		2535
p-P70S6K (Thr389)		9205
P70S6K		9202
4EBP1		9452
p-4EBP1 (Thr37/46)		2855
Tomm20		42406
COXIV		4850
Drp1		8570
parkin		4211
LAMP1		9091
GAPDH		5174
VDAC1		4661

Antibody	Company	Catalogue number
cathepsin B	Santa Cruz Biotechnology	sc-13985
cathepsin D		sc-6486
β-actin		sc-47778
p-ATGL (Ser406)	Abcam	ab135093
ATGL		ab99532
ERRa		07-662
CPT1β		ab134988
TFAM		ab131607
PINK1		ab23707
TFEB		ab2636
p-TFEB (Ser142)	Millipore	ABE1971
PGC1a	Sigma Chemical Co	SAB2500781
LAMP2	Thermo Fisher Scientific	PA1-655

Supplementary Table 2. Pathway analysis of differentially expressed genes in the gastrocnemius muscle from *SM-TRα1$^{L400R/+}$ VS. Control* mice

SM-TRα1$^{L400R/+}$ vs. Control	**Pathway ID**	**description**	**Adjusted p-value**	**Gene list**
Down-regulated	GO:0046461	neutral lipid catabolic process	0.00074	Apob|Ces1d|Cps1|Apoa2|Apoc3|Apoa1|
	GO:0032870	cellular response to hormone stimulus	0.001445	Aldob|Rhoq|Fgb|Apob|Acvr1|Nr6a1|Fyn|Eif5a|Nr3c1|Arg1|Rxrg|Egr1|Junb|Fos|Cpeb2|Myo5a|Uri1|Mef2c|Plcb1|Cacna1h|Jak2|Tsc1|Akt3|Cps1|
	GO:0032368	regulation of lipid transport	0.012703	Acsl4|Mapk9|Apoa2|Abca7|Pla2g6|Apoa1|Apoc3|Atp8a1|
	GO:0006639	acylglycerol metabolic process	0.001501	Apoa1|G6pc|Agpat1|Apoc3|Cps1|Slc27a5|Acsl4|Apoa2|Apob|Ces1d|
	GO:0032409	regulation of transporter activity	0.013862	Myo5a|Apoa2|Cbarp|Camk2d|Plcb1|Pla2g6|Mef2c|Gpd1l|Neto2|Kmt2a|Cacng7|Wnk2|
Up-regulated	GO:0005581	collagen	8.58E-08	Col4a2|Col5a2|Col11a2|Col11a1|Col1a1|Col5a1|Col5a3|Col15a1|Col6a1|Col6a3|Col12a1|Col3a1|Col4a1|Col14a1|Pcolce|Col19a1|Col6a2|Col1a2|
	GO:0071560	cellular response to transforming growth factor beta stimulus	2.31E-07	Nrep|Peg10|Aspn|Ankrd1|Smad5|Col1a1|Fbn1|Axin1|Smad2|Fn1
	GO:0046332	SMAD binding	1.33E-05	Ankrd1|Flna|Acvr1|Mef2a|Pml|Smad7|Col5a2|Zeb2|Col3a1|Tcf12|Rnf111|Col1a2|Smad2|Axin1|
	GO:0014888	striated muscle adaptation	1.20E-06	Gtf2ird1|Tead1|Tnni1|Tnnc1|Kdm4a|Atp2a2|Ppargc1a|Myh7|Cacna1s|Gsn|Tnnt1|
	GO:0060415	muscle tissue morphogenesis	1.85E-05	Rbpj|Tnnc1|Ankrd1|Tnni1|Col11a1|Rxra|Myh7|Smad7|Tbx1|Myl2|Myl3|Col3a1|

Supplementary figure legends

Supplementary Figure 1. T_3 decreased p62 in gastrocnemius muscle. Immunoblot and densitometric analysis of p62 in gastrocnemius muscle from control or T3 injected wildtype male C57BL/6 mice. T_3 was given through intraperitoneal injection at a dose of 20 µg/100g body weight for 10 consecutive days.

Supplementary Figure 2. *TRα1*^{PV} expression increased phosphorylation of 4EBP1, and decreased phosphorylation of ATGL. (A-B) Immunoblot (A) and densitometric analysis (B) showing phosphorylation of 4EBP1 and 4EBP1 in gastrocnemius muscle from *wild-type* (n=5) and *TRα1*$^{PV/+}$ (n=5) mice. (C-D) Immunoblot (C) and densitometric analysis (D) showing phosphorylation ATGL in gastrocnemius muscle from *wild-type* (n=5) and *TRα1*$^{PV+/}$ (n=5) mice. Data are shown as mean±SD.

Supplementary Figure 3. TRα1^{PV} expression decreased protein level of Drp1 but not parkin. (A-C) Immunoblot (A) and densitometric analysis (B-C) showing protein level of Drp1 and parkin in gastrocnemius muscle from *wild-type* (n=5) and *TRα1*$^{PV/+}$ (n=5) mice. Data are shown as mean±SD.

Supplementary Figure 4. T_3 did not affect Drp1 in gastrocnemius muscle. Immunoblot and densitometric analysis of Drp1 in gastrocnemius muscle from control or T3 injected wildtype male C57BL/6 mice. T_3 was given through intraperitoneal injection at a dose of 20 µg/100g body weight for 10 consecutive days.

Supplementary Figure 5. The effect of mutant TRα1 expression on protein level of CPT1β. (A) Immunoblot and densitometric analysis showing protein level of CPT1β in gastrocnemius muscle from *Control* (n=4) and *SM-TRα1*$^{L400R/+}$ (n=4) mice. (B) Immunoblot and densitometric analysis showing protein levels of CPT1β in gastrocnemius muscle from *wild-type* (n=5) and *TRα1*$^{PV/+}$ (n=5) mice. Data are shown as mean±SD.

Supplementary Figure 6. Protein levels of MHC-I and MHC2a in gastrocnemius muscle. (A) Immunoblot and densitometric analysis showing protein levels of MHC-I and MHC2a in gastrocnemius muscle from *Control* (n=4) and *SM-TRα1*$^{L400R/+}$ (n=4) mice (A) or wild-type (n=5) and *TRα1*$^{PV/+}$ (n=5) mice (B). Data are shown as mean±SD.